Effect of recombinant fibroblast growth factor 10 on the lung vasculature in a mouse model of bronchopulmonary dysplasia

Inauguraldissertation
zur Erlangung des Grades eines Doktors der Medizin
des Fachbereichs Medizin
der Justus-Liebig-Universität Gießen

vorgelegt von Gersmann, Luisa
aus Erlenbach am Main

Gießen 2025

Aus dem Fachbereich Medizin der Justus-Liebig-Universität Gießen

Cardio-Pulmonary Institute (CPI)

Gutachter: Prof. Dr. Saverio Bellusci

Gutachter: PD Dr. Klaus Deckmann

Tag der Disputation: 16.04.2026

List of Contents

1 Introduction

1.1 Bronchopulmonary dysplasia

1.1.1 Definition and epidemiology

In 1967, Northway et al. first described bronchopulmonary dysplasia (BPD) as a chronic lung injury affecting preterm infants born around 30-32 weeks gestational age (GA) associated with mechanical ventilation and high levels of inspired oxygen (Northway et al., 1967). Even today, over 50 years later, BPD remains one of the most common complications affecting prematurely born infants. Patients with BPD experience long-term sequelae, including impaired lung function, resulting in a lower quality of life. Despite advances in perinatal-neonatal health care, evidence-based treatments for preterm infants with BPD are limited, and the underlying pathophysiologic mechanisms need further investigation to elucidate the decisive connections.

BPD has been conventionally diagnosed based on oxygen needs at 36 weeks of gestational age (Jobe & Bancalari, 2001). However, this definition has been challenged by advancing respiratory support techniques in modern neonatal intensive care.
In today's world, preterm birth rates are still high at around 10% worldwide (Ohuma et al., 2023). Advanced neonatal intensive care has made it possible to treat prematurely born infants and extremely preterm infants <28 weeks can now survive. Consequently, healthcare professionals face increasing incidences of common complications of premature birth, especially BPD (Thébaud et al., 2019). In a recent review, researchers studied the global incidence of BPD in extremely preterm infants born between 24 and 28 weeks GA. The data from Europe showed that in the group of preterm infants born at ≤24 weeks GA, over 80% were suffering from BPD, while there was a lower yet variable range of the incidence (8% to 38%) reported for infants born ≥27 weeks GA (Siffel et al., 2021). This observation confirms that BPD remains a common health complication of extremely preterm infants, therefore the need for effective therapeutic treatments is larger than ever.

Regarding histological features, old BPD was characterized as generalized airway and vascular damage with diffuse fibrosis, whereas new BPD is marked by simplified alveolarization and remodeling of vasculature due to paradigm shift in respiratory support

(Kalikkot Thekkeveedu et al., 2017). Despite decades of research on BPD focusing on the impairment of the airways, the pathomechanisms of vascular dysmorphy and remodeling as well as its association with pulmonary hypertension (PH) have not been fully clarified (Arjaans et al., 2018). Several studies based on echocardiography have revealed pulmonary and cardiac impairments in extremely preterm infants, including heightened pulmonary pressure and resistance that persist into early adulthood (Thébaud et al., 2019). Neumann et al. demonstrated that echocardiographic measurements and right ventricular function have prognostic value. They can be used to predict the risk of developing BPD and the likelihood of death in very preterm infants (Neumann et al., 2021).

1.1.2 Risk factors for the development of bronchopulmonary dysplasia

The development of BPD is multifaceted and connected to various genetic and environmental risk factors. The most significant independent risk factor is extreme prematurity, defined as a gestational age of less than 28 weeks (Dankhara et al., 2023). Pre-, peri- and postnatal events, such as maternal smoking, chorioamnionitis, pregnancy-induced hypertension (PIH), intrauterine growth restriction, and sepsis have been demonstrated to contribute to the development of BPD as well. Fetal growth restriction affects 5-10% of all pregnancies worldwide and can result in extremely low birth weight (ELBW), which makes newborns especially susceptible to BPD and severe complications of this chronic lung disease, namely associated pulmonary hypertension (BPD-PH) (Bui et al., 2017; Sehgal et al., 2019). Furthermore, various biomarkers have been found to be associated with BPD. The underlying mechanisms are not yet fully comprehended and are the focus of ongoing research (Dankhara et al., 2023).

Oxygen toxicity plays a crucial role in the development of BPD. Premature infants are particularly vulnerable to oxidative stress due to their underdeveloped lung defense mechanisms. Reactive oxidant species (ROS) can fuel inflammation leading to the release of inflammatory substances and mediators. Consequently, alveolar simplification and rarefaction of pulmonary vessels often occur, exacerbating the impairment of lung development in BPD (Dankhara et al., 2023). Figure 1 illustrates various factors contributing to the development of BPD, including genetic factors, antenatal and

postnatal stress, as well as extreme prematurity as a significant risk factor. Furthermore, it describes the impact of persistent respiratory disease and its associated consequences.

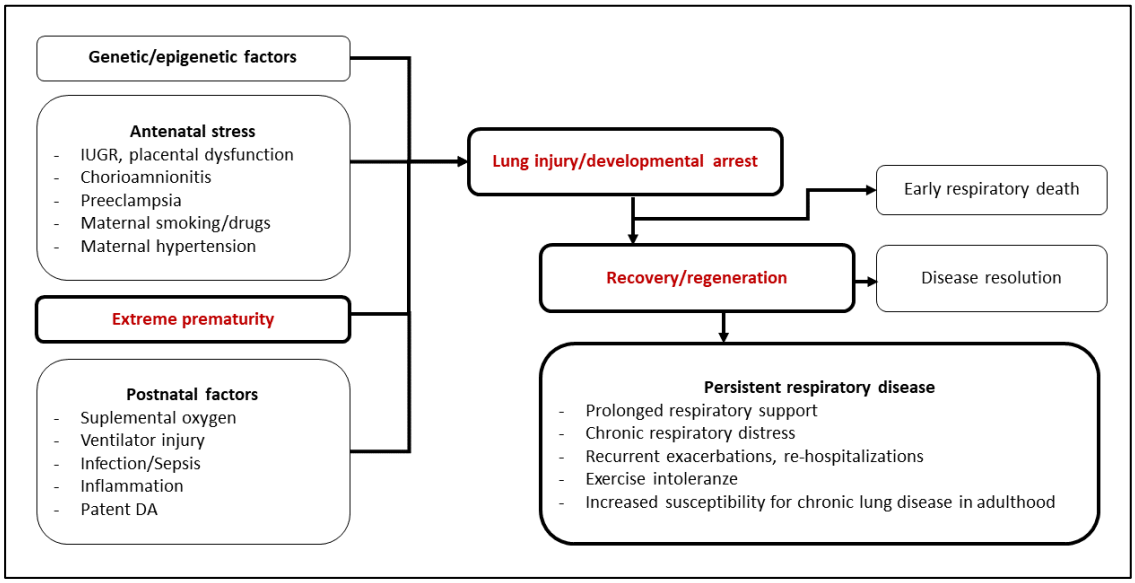

Figure 1: **Algorithm for pathogenesis of BPD** (Modified from: Abman et al., 2017).
DA: ductus arteriosus; IUGR: intrauterine growth restriction

1.1.3 Currently available therapeutic options and prognosis

Managing extremely preterm infants remains a challenge as postnatal interventions can have both positive and negative effects. Since lung maturation accelerates with abundant surfactant production after 35 weeks gestational age, children born extremely premature (≤28 weeks) encounter significant respiratory difficulties.

Essential medical interventions for supporting preterm infants with immature lungs include mechanical ventilation, and using oxygen to facilitate adequate gas exchange (Haggie et al., 2020; Schittny, 2017). In the initial moments of life, it's preferable to prioritize non-invasive respiratory support over intubation and ventilation to minimize the risk of mechanical lung injury. Additionally, exogenous surfactant therapy can aid lung maturation and offset the absence of natural surfactant during the early stages of lung development, ultimately enhancing the prognosis for preterm infants.

Between the point of reaching viability (23-24 weeks' gestation) and the acceleration of lung maturation due to increased surfactant production (>34+0 weeks' gestation), glucocorticoids can be administered prepartum if premature birth is imminent. This treatment leads to faster maturation of the surfactant-producing type II alveolar epithelial cells (AT2). Postpartum, corticosteroids are used to reduce inflammation and thereby lower the infant`s risk of mortality (Thébaud et al., 2019). To address BPD-related vascular damage and associated pulmonary hypertension, inhaled nitric oxide (iNO) can be administered, leading to relaxation of smooth muscle cells in the pulmonary vessels and vasodilation, thus reducing pulmonary pressure. It's important to note that current therapies mainly focus on managing symptoms, and there is no standard treatment targeting the root causes of BPD (Berkelhamer et al., 2018).

Managing short-term BPD presents a significant challenge in balancing oxygen levels to minimize toxicity while ensuring adequate oxygen saturation in newborns. While the mentioned therapeutic options can improve outcomes and quality of life for premature infants, there is a high demand for new targeted therapies. Long-term treatment of BPD remains an unsolved issue, as damage sustained in the first few weeks of life is often irreversible, leading to lifelong impairment. The need for interdisciplinary care teams for chronic complex lung disease is crucial, however, such structures and knowledge are not universally available. (Thébaud et al., 2019).

For many patients, BPD becomes a lifelong challenge that brings about significant social and economic burdens. Up to 50% of infants with BPD undergo rehospitalization before their second birthday, often due to infections caused by respiratory viruses like influenza virus or respiratory syncytial virus. Furthermore, the risk of asthma-like symptoms remains elevated during the preschool and school-age years compared to other children in the same age group (Thébaud et al., 2019). Around 25% of infants with moderate to severe BPD develop BPD-related pulmonary hypertension, a condition linked to increased rates of morbidity and mortality (El-saie et al., 2024; Hansmann et al., 2021).

1.2 Development of the lung

1.2.1 The physiological stages of lung development

Understanding how disruptions in lung development can cause chronic lung diseases such as BPD and associated pulmonary vascular disease requires an exploration of the physiological stages of lung growth. Human lung development can be divided into three main periods and four histologically distinguishable stages. These periods include the embryonic phase, which involves lung organogenesis and the formation of major airways and pleura. Subsequently, the fetal phase comprises the pseudoglandular, canalicular, and saccular stages, resulting in branching morphogenesis. Finally, alveolarization and microvascular maturation occur from 36 weeks preterm through young adulthood, constituting the postnatal stage of lung development. To explain the mouse model used in this study, the corresponding time points in mouse lung development will also be discussed.

During human pregnancy, the embryonic and pseudoglandular stages occur from week 4 to 17, which corresponds to embryonic day (E) 9.5-E16.5 in mice. Following these stages, the canalicular stage takes place from week 17 to 26 in humans (E16.5-E17.5 in mice), then the saccular stage from weeks 26 to 36 (E17.5-postnatal day (PN) 5 in mice), and finally, the alveolar stage from the last weeks of pregnancy through the 8th year of life (PN5-PN30 in mice). The classification of these stages is based on morphological characteristics, and it's important to note that regional differences may lead to temporal variations in the developmental processes, particularly between central and peripheral lung regions (Chao et al., 2020; Schittny, 2017).

Over the past few years, there has been growing evidence supporting the pivotal role of pulmonary vessels in lung development. Contrary to previous assumptions, the pulmonary vasculature does not passively accompany airway development but rather facilitates alveologenesis (Chao et al., 2020; Thébaud et al., 2005). Following the differentiation of mesenchymal cells, the initial pulmonary vessels are generated through vasculogenesis, which is the process of de novo formation of vessels. These vessels create a network around the lung buds within the mesenchymal tissue, with each bud being enveloped by a vascular plexus. As the canalicular stage progresses, the double-layered capillaries proliferate, bringing the alveolar epithelium and the adjacent endothelium

basement membranes into closer proximity through epithelial differentiation, thus forming the future air-blood barrier. Subsequently, during the saccular stage, the pulmonary vessels in the mesenchyme establish a three-dimensional network that increases in density. This process of developing new vascular structures from existing ones is referred to as angiogenesis (Ochoa-Espinosa & Affolter, 2012). In the canalicular stage of lung development, a crucial step is the start of surfactant production by AT2 cells. Surfactant reduces surface tension in the alveoli, making it easier for them to inflate. Reaching this stage of development is particularly important for premature infants, as it allows them to develop as much gas-exchanging surface area as possible before birth. During the following saccular stage, the gas exchange region expands, and single capillary layers form, reducing the distance of the air-blood barrier. When a baby is born at full term, the blood-air interface is almost fully formed. However, premature babies must complete this process after birth. In humans, saccular development begins before birth and progresses to alveolarization around 36 weeks after birth. In mice, this process occurs after birth (Surate Solaligue et al., 2017; Schittny, 2017). See Figure 2 for a summary of the stages of lung development in humans.

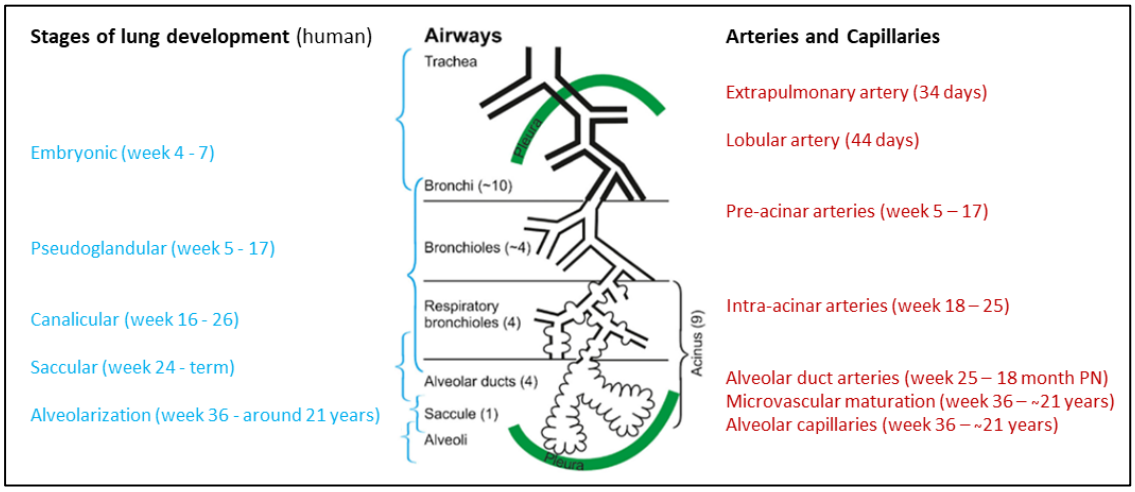

Figure 2: **Development of airways (black) and arteries (red) during different stages of lung development (blue)** (Modified from: Schittny, 2017).
Pre-acinar arteries grow by vasculogenesis, intra-acinar arteries are formed through angiogenesis

1.2.2 Multicellular crosstalk and microenvironment during lung development

Communication between epithelial and mesenchymal cells is essential throughout the complex process of lung development. This crosstalk is partly regulated by signaling factors secreted from the epithelial or mesenchymal compartments. Diffusible ligands from the mesenchyme move to the adjacent epithelium through a suitable receptor. In the epithelium, this process activates target genes and leads to the release of other signaling molecules. These ligands, in turn, can have activating or suppressing effects on the mesenchyme, creating negative feedback loops (Jones et al., 2021). Key factors in alveolarization include fibroblast growth factor 10 (FGF10), bone morphogenic protein-4 (BMP4), transforming growth factor beta (TGF-ß), and others, which initiate and regulate branching morphogenesis (Schittny, 2017).

The development of the lungs involves both direct regulatory mechanisms during alveolarization and several indirect processes related to the extracellular matrix (ECM) surrounding the cells. This intricate network of molecules, including proteins like collagen and glycoproteins secreted by mesenchymal and epithelial cells, plays a crucial role in organogenesis. Additionally, the ECM has the potential to adapt to different conditions through constant remodeling processes (Jones et al., 2021). Sufficient gas exchange in the lungs relies on an extensive network of blood vessels, which, together with the alveoli, forms the blood-air barrier. During vasculogenesis, endothelial progenitor cells from the mesoderm form a network of individual angioblasts, serving as the starting point for the development of the vascular network (Ochoa-Espinosa & Affolter, 2012).

During the development of pulmonary vessels, vascular endothelial growth factor A (VEGF-A) and its receptor (VEGFR2) are essential for initiating and regulating vasculogenesis and angiogenesis. Mesenchymal cells are the initial source of VEGF during early lung development, while later, AT2 cells from the airway epithelium take over this role. VEGF signaling also facilitates the attraction of endothelial and epithelial cells, ensuring synchronized vasculogenesis and the branching of airways, which is vital for the creation of a functional capillary-alveoli network. Additionally, α-smooth muscle actin positive cells (VSMCs) derived from the mesenchyme are part of the tunica media

of larger vessels, while in smaller vessels, VSMCs transform into pericytes that encircle the capillaries and regulate microvasculature and alveolar development.

Another marker of angiogenesis and vascular permeability is platelet endothelial cell adhesion molecule 1 (PECAM1) also known as cluster of differentiation 31 (CD31). It is highly expressed on endothelial cells and plays a critical role in maintaining the integrity of the endothelial barrier (Chao et al., 2020; Jones et al., 2021). Additionally, a recent study underlined the importance of claudin 1 (CLDN1), an integral membrane protein and component of tight junction strands, for intercellular barrier function during lung development (Hou et al., 2024).

1.2.3 Differences between proximal and distal areas of the lung

The lung develops from proximal (the stalk) to distal (the tips) areas. In a recent review Jones et al. describe differences between the cellular composition of proximal and distal areas. Proximal epithelial cells are relatively differentiated, while distal areas contain airway progenitor cells. They also highlight higher FGFR2b signaling at the tips of the airways and a higher concentration of FGF10 (Jones et al., 2021). This supports the idea that distal areas have more potential for development and regeneration but are also more susceptible to harmful influences. Additionally, the proximity of distal airway epithelium and the surrounding vascular plexus is crucial. It has been demonstrated that FGF10 from the mesenchyme results in higher levels of VEGF in the distal epithelium (Scott et al., 2010). Regarding pulmonary vasculature, small vessels in the distal lung are particularly affected by excessive muscularization in conditions like pulmonary hypertension and BPD (Chao et al., 2020). It’s important to note that different lung areas consist of different cells and tissues and react differently to endogenous and exogeneous influences. Therefore, it's reasonable to study proximal and distal areas of the lung separately to understand local changes in chronic lung diseases such as BPD.

1.3 Pathogenesis of bronchopulmonary dysplasia and associated pulmonary hypertension

1.3.1 Pulmonary vasculature in bronchopulmonary dysplasia

Premature birth interrupts the complex process of alveolarization and vascularization before completion, leading to damage that often requires medical treatment. Oxygen toxicity, pulmonary inflammation and trauma from mechanical ventilation contribute to histopathological changes such as a decreased number and complexity of alveoli, as well as dysfunctional and aberrant pulmonary vascularization, which leads to inadequate gas exchange (Haggie et al., 2020; Schittny, 2017). Lungs of children suffering from BPD show a rarefication of pulmonary vasculature and thickening of the smooth muscle layer in the arteries, leading to increased pulmonary blood pressure. Previous studies have demonstrated that decreased vascular endothelial growth factor mRNA, which codes for a proangiogenic factor in the lungs, contributes to impaired vascular growth in infants dying from BPD. Furthermore, lung samples of these patients showed decreased expression of Pecam1, suggesting a decreased relative number of endothelial cells in these patients due to impaired vascular development (Bhatt, 2001). Another study describes simplification of the alveoli, like that seen in BPD, after blockade of *Vegf* in newborn rats. These results indicate that the pulmonary vessels have a significant influence on the airways and that this may be a potential therapeutic target (Thébaud et al., 2005). Indeed, it has become increasingly appreciated that the remodeling of the pulmonary vasculature takes a key role in the pathology of BPD. Vascular abnormalities not only affect blood flow but also impact heart function, often causing pulmonary hypertension, which is frequently associated with BPD (Chao et al., 2020).

Research suggests that the development of the lung's blood vessels is closely linked to the development of the airways. Recent studies pointed out that one of the main vessel-associated challenges in BPD is the pulmonary vascular remodeling which leads to the proliferation of existing vascular smooth muscle cells around already muscularized vessels as well as de novo muscularization of previously non-muscularized vessels. A distal extension of the muscular arterioles suggests that the distal areas of the lung are most affected by the arrested microvascular development, while the effects on airway branching remain to be uncovered. Therefore, distal regions require special attention in studies on lung microvasculature (Chao et al., 2020; Sehgal et al., 2019).

Another study by Lazarus et al. showed that after ablation of the pulmonary vessels, the spatial orientation of airway branching was dramatically disturbed, independent of perfusion. There was an incomplete rotation of the bronchi and an overall reduced number of bronchi. This suggests that vascular endothelial cells play a significant role in epithelial-mesenchymal cross-talk during airway development (Lazarus et al., 2011).

1.3.2 Bronchopulmonary dysplasia associated pulmonary hypertension

Infants with severe forms of BPD are particularly susceptible to pulmonary hypertension, which is associated with an increased risk of mortality (Arjaans et al., 2018). Since the description of "new" BPD in 1999, the involvement of the pulmonary vasculature and its contribution to the pathophysiology of chronic lung disease has become more relevant. In this context, Mourani and Abman pointed out that pulmonary vascular impairment may not always manifest clinically as pulmonary hypertension. Instead, affected patients may exhibit symptoms suggestive of pulmonary vascular disease (PVD). This term encompasses a range of abnormalities in the vascular system that can occur in the lungs of infants with BPD, including persistent oxygen dependency, decreased performance, and susceptibility to lung infections (Mourani & Abman, 2013). Further clinical studies have shown that the diagnosis of early pulmonary vascular disease is linked to the development of BPD and late PH (Mourani et al., 2015). In these patients, there is a decrease in pulmonary blood vessel growth and structural and functional abnormalities in the lung's vascular system. As a result, less lung area is available for gas exchange, and affected children may develop pulmonary hypertension (Mehler et al., 2017).

1.4 The role of fibroblast growth factors during lung development and bronchopulmonary dysplasia pathogenesis

1.4.1 The fibroblast growth factor family

Fibroblast growth factors (FGFs) are small proteins with an average weight of 20 kDa, that function as growth factors in a paracrine or autocrine manner upon secretion. There are 22 members of the FGF family, categorized into seven subfamilies, which regulate many different biological functions. FGFs from the FGF11 subfamily exert intracellular effects, while those from the endocrine FGF19 subfamily act as hormones, being secreted to the bloodstream. The remaining FGFs operate by specifically binding and activating fibroblast growth factor receptors 1-4 (FGFR1-4) (Maddaluno et al., 2017).
FGF-signaling is transmitted by the formation of FGF-HSPG-FGFR ternary complexes (HSPG: heparan sulfate proteoglycans). The binding of FGF-HSPG-complexes to FGFRs initiates dimerization and phosphorylation of tyrosine residues within the FGFRs intracellular domain, leading to the activation of additional signaling pathways that regulate cell differentiation and migration (Finch et al., 2013; Maddaluno et al., 2017; Prudovsky, 2021).

1.4.2 Characteristics of the fibroblast growth factor 10 pathway

FGF10 is part of the canonical FGF7 subfamily and binds to the transmembrane tyrosine kinase receptor FGFR2b, which is primarily expressed by epithelial cells and plays a crucial role in embryonic development and tissue regeneration following injury (Finch et al., 2013). FGF10 is among the earliest markers in the lung mesenchyme, and prior research has highlighted its essential role in lung development, particularly in the formation of alveoli and the development of the pulmonary vasculature. The associated receptor FGFR2b is expressed by the lung epithelium, and binding of FGF10 facilitates intercellular communication between mesenchymal and epithelial cells (Chao et al., 2019). In addition to FGF10, other members of the FGF7 subfamily, such as FGF1, FGF7 and FGF22, also bind to the FGFR2b variant of the fibroblast growth factor receptor. Both FGF10 and FGF7 have the highest specificity for the receptor and are secreted by mesenchymal cells. When investigating the effects of FGFR2b signaling, it is crucial to consider the potential implications for the entire FGF7 subfamily. Notably, FGF7 is upregulated following tissue injury, indicating its significant role in the repair processes

and alleviation of lung injury, alongside FGF10 (Finch et al., 2013; Maddaluno et al., 2017).

The expression of FGF10 occurs in two distinct waves during lung development, at the beginning and at the end of the pseudoglandular stage (El Agha et al., 2014). FGF10 is essential for alveolar development, promoting the formation of alveolar epithelial cells. It stimulates the differentiation of bronchial epithelial stem cells into alveolar type 2 (AT2) cells, which are vital for gas exchange and surfactant production. This process is mediated through FGF10 binding to its receptor FGFR2B, initiating signalling pathways that drive alveolar epithelial regeneration (Yuan et al., 2019). Beyond its role in alveolar development, FGF10 influences pulmonary vascularization. Studies have shown that FGF10 overexpression can restore lung alveolar and vascular structures in mice with emphysema and pulmonary hypertension induced by cigarette smoke and elastase. This suggests that FGF10 has the potential to repair both alveolar and vascular components of the lung, highlighting its therapeutic promise for lung diseases characterized by alveolar and vascular damage (Hadzic et al., 2023). Notably, studies have shown that FGF10 expression is reduced in human BPD due to inflammatory signals, indicating the potential role of this fibroblast growth factor in the pathophysiology of BPD (Chao et al., 2019). Furthermore, Chao et al. demonstrated that *Fgf10* deficiency leads to lethality in a mouse model of BPD (Chao et al., 2017). In line with these findings, Jones et al. revealed that FGF10 signaling through its receptor FGFR2b regulates certain crucial biological processes during early pseudoglandular development, which are essential for proper lung organogenesis (Jones et al., 2019).

While the crucial role of FGF10 in airway branching processes has been well known for a long time, recent studies have focused on its impact on pulmonary vasculature and the underlying mechanisms. The lung vasculature develops near the airway epithelium, suggesting that endothelial and epithelial cells communicate extensively. Previous studies have found that decreased secretion of FGF10 from the mesenchyme is due to increased levels of specific MicroRNAs and feedback loops with sonic hedgehog (SHH) and Sprouty2 (SPRY2). This leads to the downregulation of VEGFA, resulting in reduced activation of the associated receptor VEGFR2 and impaired angiogenesis (Chao et al., 2020).

Additionally, a recent paper by Chao et al. suggests that defective FGF10 signaling can lead to vascular defects in individuals with BPD. As a result, recombinant FGF10 may hold promise as a potential therapeutic option in the future. In a mouse model of BPD, the researchers observed a reduced number of blood vessels and abnormal vascular muscularization in the lungs of *Fgf10*-deficient mice exposed to hyperoxia (Chao et al., 2019). Previous studies on rats by Scott et al. showed that FGF10/FGFR2b/SPRY2 signaling is involved in the activation of a complex that regulates VEGFA production and secretion from the airway epithelial cells (Scott et al., 2010). Another publication by Walker and Land highlights the role of FGF10 in regulating VEGFA expression through mTORCH1-HIF-1alpha (Walker & Land, 2018). Ramasamy et al. demonstrated decreased expression of PECAM in the lungs of *Fgf10* hypomorphic mice, indicating a link between FGF10 signaling and vascular development (Ramasamy et al., 2007). These findings underscore the importance of FGF10 for the development of the pulmonary vasculature and suggest that decreased FGF10 levels may contribute to vascular defects, while FGF10 as a potential therapeutic agent could promote vascular recovery (Chao et al., 2019; Jones et al., 2021).

1.4.3 Fibroblast growth factor 10 and inflammation in bronchopulmonary dysplasia

Several studies have investigated the association between decreased levels of FGF10 and the development of BPD and BPD-PH in patient biosamples. Benjamin et al. found decreased expression of FGF10 in the lungs of infants with BPD compared to age-matched controls (Benjamin et al., 2007). The impaired FGF10 signaling pathway not only affects lung growth but also plays a key role in the inflammatory processes that drive the pathogenesis of BPD. Previous studies have shown that levels of cytokines and chemokines are altered in BPD, leading to a proinflammatory state. Persistent inflammation disrupts cell-cell communication, ultimately contributing to various types of lung damage. Growth factors such as FGF10 and VEGFA have anti-inflammatory effects and regulate inflammatory processes after injury to support recovery.

In BPD, the levels of these anti-inflammatory molecules are reduced, indicating an overall diminished capacity for regeneration. Chao et al. hypothesized that decreased FGF10 expression could further lead to dysregulation of genes responsible for vascular barrier function and airway inflammation (Chao et al., 2019; Marega et al., 2023).

Another study by Yuan et al. on microRNA-421 inhibition demonstrated increased inflammation and apoptosis in lung tissue after decreased FGF10 expression (Yuan et al., 2019). These findings collectively suggest that decreased levels of FGF10 are associated with the development of BPD, highlighting its potential as a therapeutic target for these conditions.

1.4.4 Therapeutic potential of fibroblast growth factor 10 in bronchopulmonary dysplasia

A recent study conducted in our laboratory demonstrated that the administration of rFGF10 can trigger de novo alveologenesis in a BPD mouse model (Taghizadeh et al., 2022). However, further exploration is needed to understand the impact of rFGF10 as a potential therapeutic agent on lung vasculature. Chao et al. observed a significant reduction in the number of pulmonary blood vessels in the lungs of *Fgf10* deficient mice under hyperoxia compared to the control group (Chao et al., 2019). These findings suggest that decreased FGF10 activity contributes to vascular defects, which are recognized as a key feature of BPD. Additionally, the effects of FGF10 expression on the vascular system can be categorized into two groups: first, its influence during vascular development, and second, its effects on repair after vascular damage, particularly in the context of endothelial proliferation (Chao et al., 2019). These discoveries offer valuable insights into the pathways involved in BPD pathogenesis and associated PVD, laying the groundwork for further research into FGF10 treatments and its potential role in developing therapies for BPD patients.

2 Aims of the current study

Previous research has highlighted the significant role of FGF10 in the proper development of pulmonary airways. While the connection between impairment of the vascular system and BPD is generally recognized, there has been limited focus on the underlying mechanisms and the specific impact of FGF10 on the pulmonary vasculature. Despite the evident link between pulmonary vascular development and BPD-related long-term complications, there remains a lack of comprehensive understanding in this area, as well as the potential therapeutic applications of FGF10. Therefore, our current study uses a mouse model of BPD to investigate the effects of hyperoxia-induced lung injury, a well-established animal model to induce lung alterations similar to the ones found in BPD, specifically on the lung's vascular system (Fig. 3).

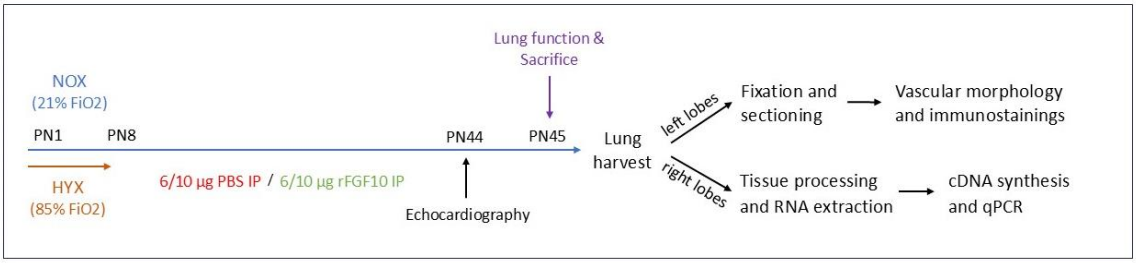

Figure 3: Schematic description of experimental design

NOX: Normoxia; HYX: Hyperoxia; PBS: Phosphate-buffered saline; rFGF10: recombinant fibroblast growth factor 10; PN: postnatal; IP: intraperitoneal; qPCR: quantitative real-time RT-PCR

In addition, we investigated the effects of recombinant FGF10 treatment on pulmonary vessels and examined whether rFGF10 could enhance the prognosis of experimental mice, thereby exploring the potential of this recombinant protein as a therapeutic agent for BPD. Prior to lung harvest, we assessed the impact of the experimental conditions on organ functions by conducting echocardiographic measurements and lung function analyses, well-established methods for monitoring BPD and BPD-PH in the clinical setting (Mehler et al., 2017).

By selecting PN45 as our timepoint for lung harvest, we were able to study the lungs during the early stage of adulthood. There is currently no similar study specifically focusing on investigating the long-term effects of hyperoxia and recombinant FGF10 in a mouse model of BPD into adulthood. Our research aims to provide a more

comprehensive understanding of BPD in later stages of lung development and the role of the pulmonary vasculature at this stage. Additionally, we intend to explore potential differences in the impact of hyperoxia-induced lung injury and our FGF10 treatment in various regions of the lung by comparing proximal and distal areas of the pulmonary vasculature during our experiments.

In this study, our primary objectives are to address the following key questions:

1. Can exposure to hyperoxia during the first week of life result in detectable changes in the pulmonary vascular system at PN45 in our mouse model of BPD?
2. What impact does rFGF10 treatment have on the restoration of the pulmonary vasculature following hyperoxia exposure?
3. Are certain lung regions more affected by hyperoxia-induced injuries and rFGF10 treatments than others?

3 Material and methods

3.1 Study approval and generation of mice

All animal experiments were approved by the Federal Authorities for Animal Research of the Regierungspräsidium Giessen, Hessen, Germany, protocol numbers G29/2020-No. 994_GP and G85/2019-No. 986_GP. We received pregnant C57BL/6J wildtype mice at embryonic day (E) 14 from Jackson through Charles Rivers Laboratory, Germany. According to the guidelines of the institution the mice were housed by the Animal Care and Veterinary Service of the Justus-Liebig-University Gießen, Hessen, Germany.

3.2 Hyperoxia-induced lung injury: The bronchopulmonary dysplasia mouse model

The newborn pups were randomized into three groups: one control group (normoxia (NOX)) and two experimental groups (hyperoxia (HYX), treated with PBS-Buffer or recombinant FGF10 (rFGF10)). The newborn pups from the two experimental groups were put into an hyperoxia chamber with an atmosphere of 85% fraction of inspired oxygen (FiO_2) for 8 days (Postnatal day (PN) 0 - PN8). At the same time the animals from the control group were held under room air with 21% FiO_2. The mother animals were rotated every 24 hours between NOX and HYX to minimize the impact of oxygen toxicity on the adult mice and avoid changes in nursing behavior. All animals received food and water ad libitum. After PN8 all mice were brought back to normoxic conditions. The following experimental treatment was carried out in three rounds: Between PN8 and PN14 the pubs from the hyperoxia groups received the first 4 intraperitoneal injections with 6 µg rFGF10 or PBS each. In the second round (PN22-PN28) the same procedure was performed with an increased concentration of rFGF10 (10 µg), to adjust the amount of active substance to the increasing weight of the young animals at this timepoint. This treatment was repeated in the last round (PN36-PN42). Figure 4 shows the experimental scheme of the BPD mouse model.

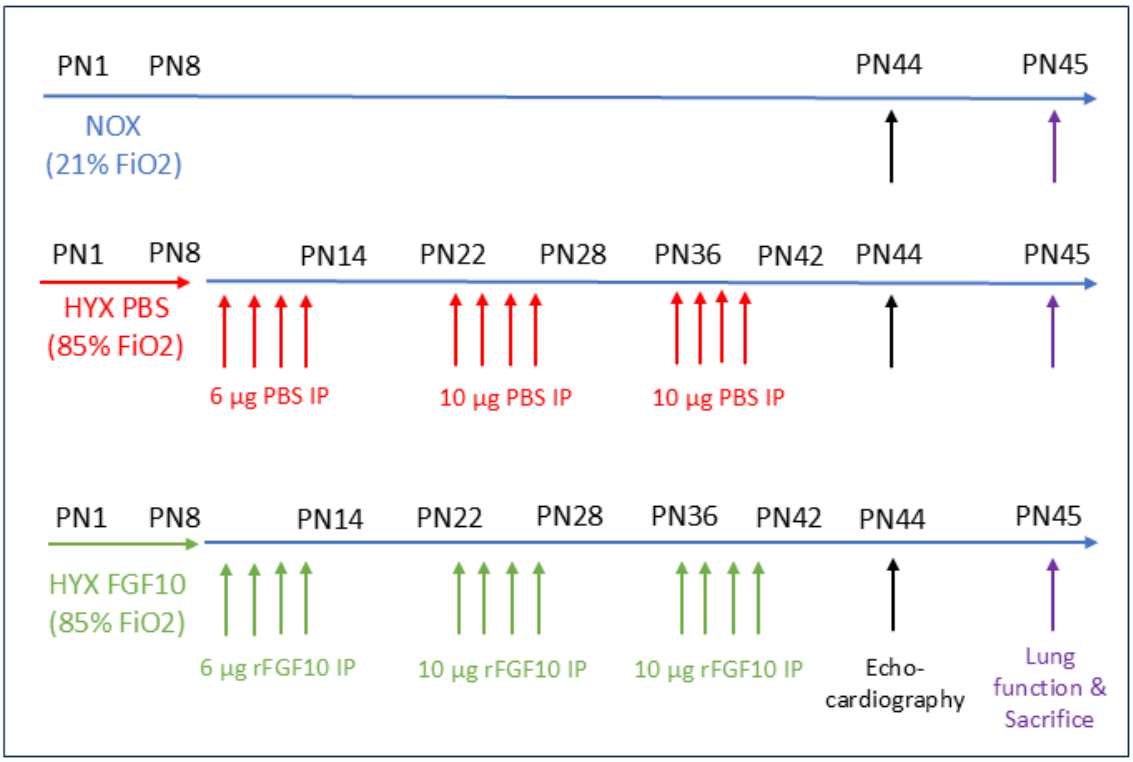

Figure 4: Experimental scheme of the BPD mouse model

PN: postnatal; IP: intraperitoneal; NOX: Normoxia; HYX: Hyperoxia; PBS: Phosphate-buffered saline; rFGF10: recombinant Fibroblast growth factor 10

3.3 Echocardiography

The echocardiographic measurements were performed by Dr. Simone Kraut on PN44 before lung harvest. Mice were put under anesthesia using isoflurane (1.5% v/v) and placed on a heating table to maintain a core temperature of 37°C, which was measured via rectal probe. The images were generated using Vevo 770 high-resolution imaging system via a 30-MHz RMV-707B scanning head (VisualSonics, Toronto, Canada). In the right parasternal long-axis view the free wall thickness of the right ventricle (RVWT) was measured. After the apical four-chamber view was set, the right ventricular internal diameter (RVID) was measured in the middle third of the right ventricle as maximal transverse diameter during end-diastole. To estimate the function of the right ventricle, the tricuspid annular plane systolic excursion (TAPSE) was measured. The images were afterwards analyzed by one observer who was blinded regarding the distribution of the mice to the different groups (Veith et al., 2020).

3.4 Lung function measurement

The anesthesia was performed by Kerstin Goth on PN45 by injecting a solution of 1.2 µl/g body weight of ketamin 10% and 0.6 µl/g body weight of dormitor (1mg/ml) into the peritoneum. To make sure the anesthesia was deep enough, the mice were pinched into the toes. When they did not show a reaction to this pain anymore (about 15 min after the induction), a small incision on the skin and fascia was made above the larynx and the trachea was uncovered from the surrounding muscle. Another horizontal incision was made to intubate the mice. After the connection of the ventilation tube with the SCIREQ Oszillationplethysmograph (FlexiVent, Scireq Inc, France, **Fig. 5**) we started the lung function measurement. Five consecutive measurements (mean values) of compliance, resistance and elastance were made while the airway pressures were registered continuously.

Figure 5: ScireQ Oszillationplethysmograph (Scireq, FlexiVent) for lung function measurement
The anesthetized and intubated mice were placed on a styrofoam box lying on the back to reach the height of the connection unit of the oszillationplethysmograph (red arrow). The intubation tube was connected with the oszillationplethysmograph and the machine automatically measured the lung function.

3.5 Lung harvest

Mice were sacrificed at PN45. Sternotomy was performed to open up the chest cavity. Intracardial perfusion was performed with injection of phosphate-buffered saline (pH 7.0) from the right ventricle to the left ventricle at a vascular pressure of 20 cm H_2O to remove blood from the lungs. Then the right lobe was clipped and removed for further procedure. The remaining left lobe was perfused with 4% PFA via the trachea and tied up with a string to keep the PFA in the lung. The left lobe was removed and placed in 4% PFA over night at 4°C.

3.6 Fixation of the left lobes of the lungs

The following day the samples were placed in PBS 1x overnight at 4°C. On the third day the samples were put into ethanol 30%, 50% and 70%, 3 hours each, followed by ethanol 100% overnight, all at 4°C, for progressive dehydration. In the next step the lobes were placed in Xylol at room temperature for about 40 min on a shaker until they became transparent. To fix the samples in paraffin (Leica, Surgipath Paraplast Plus, Cat. No. 39602004) they were first put into a 1:1 Xylol-paraffin mix for 2 hours at 60°C and afterwards into pure paraffin at 60°C overnight. Finally, the left lobes were embedded in paraffin blocks with a Leica embedding machine (Leica EG1150C). The blocks were stored at 4°C until they were sectioned at 3 µm thickness with a Leica manual microtome (Leica RM2235).

3.7 Tissue processing of the right lobes and RNA extraction

While the left lobes of the lungs were used for morphology and immunostainings, the right lobes underwent further procession for RNA extraction. After lung harvest the tissue of the right lobes was placed in Eppendorf tubes filled with 700 µl RLT lysis buffer (QIAzol lysis reagent (Qiagen GmbH, Hilden, Germany)). Next the tissue was homogenized in GentleMACs Dissociater (Miltenyi Biotech, Bergisch Gladbach, Germany) for 1 min and afterwards centrifuged at maximum speed for 3 min. The resulting supernatant was pipetted and used for the following RNA extraction, which was performed using the RNeasy Mini Kit (Qiagen, Hilden, Germany) following the manufacturer`s protocol described in the following section.

One volume of 70% ethanol was added and mixed well with the sample. Next 700 µl of the sample were transferred to a RNeasy Mini spin column placed in a 2 ml collection tube. After the lid was closed the tube was centrifuged (≥ 8000 x g, 1000 rpm, 15 s) at room temperature and the flow-through was discarded. This step was repeated using the remaining sample. 700 µl of Buffer RW1 were added to the RNeasy column and the closed column was centrifuged (≥ 8000 x g, 1000 rpm, 15 s) before the flow-through was discarded. In the following step 500 µl Buffer RPE were added to the RNeasy spin column and again centrifuged for 15 s followed by the discard of the flow-through. After that 500 µl of Buffer RPE were added and centrifuged (≥ 8000 x g, 1000 rpm, 15 s). This step was repeated, and the centrifugation was extended to 2 min. The RNeasy spin column was transferred to a new 2 ml collection tube and centrifuged at full speed for 1 min to dry the membrane. Next, the RNeasy spin column was placed in a new 1.5 ml collection tube where 30 µl RNase-free water were pipetted onto the RNeasy column membrane. Afterwards the column centrifuged again (≥ 8000 x g, full speed, 1 min) to elute the RNA for further processing. Finally, the concentration of RNA in the sample was estimated with the ND-1000 spectrophotometer (Nanodrop, Montchanin, Germany) using 1 µl RNA for each measurement.

3.8 cDNA synthesis and quantitative real-time RT-PCR

The previously extracted RNA was reverse-transcribed using the QuantiTect Reverse Transcription Kit (Qiagen, Hilden, Germany) according to protocol (cDNA synthesis). RNase free water was added until a volume of 12 µl was reached. The prepared solution was mixed with 2 µl gDNA wipeout. The mixture was incubated for 2 min at 42°C (Step 1 of the LightCycler, PEQstar2x, PEQlab) and afterwards placed on ice.

In the meanwhile, the reverse transcription Master Mix was prepared: (1 µl RT Quantiscript Reverse Transcriptase + 4 µl Quantiscript RT Buffer + 1 µl RT Primer Mix) * (number of needed reactions + 2). 6 ul of Master Mix were added to the 14 µl RNA followed by an incubation of 30 min at 42°C and finally incubated for 3 min at 95°C to inactivate the Quantiscript Reverse Transcriptase (Step 2 of the LightCycler, PEQstar2x, PEQlab). The resulting cDNA was then diluted (1:10, up to 200 µl) and stored or proceeded with qPCR.

The cDNA was diluted to a concentration of 5 ng/µl. We designed the required primers for qPCR using the webtool https://www.ncbi.nlm.nih.gov/tools/primer-blast/ of the National Center for Biotechnology Information (NCBI). PowerUp SYBR Green qPCR SuperMix-UDG (invitrogen/life technologies, 1655057, Carlsbad, CA) was used for qPCR with a Roche LightCycler 480 machine. Samples were run in duplicates and GAPDH was used as a reference gene. Table 1 shows the primer sequences used for qPCR.

Gene	**Forward sequence**	**Reverse sequence**
Vegfa	AAA AAC GAA AGC GCA AGA AA	TTT CTC CGC TCT GAA CAA GG
Kdr	TCC ATG TGA TCA GGG GTC CT	GCA CAA CAG GGA CAC ACT CT
Fgf7	GAGAGGCTCAAGTTGCACGA	CGGTTGCTCCTTGACTTTTGT
Cldn1	GCCATCTACGAGGGACTGTG	CCCCAGCAGGATGCCAATTA
Pecam1	GAGCCTCACCAAGAGAACGG	CTCTTCTCGGGACATGGACG

Table 1: **Primer sequences (forward/reverse) for qPCR.**
Vegfa: Vascular endothelial growth factor a; *Kdr*: Kinase insert domain receptor (also known as: Vascular endothelial growth factor receptor 2); *Fgf7:* Fibroblast growth factor 7; *Cldn1*: Claudin 1; *Pecam1*: Platelet and endothelial cell adhesion molecule 1.

3.9 Immunostaining

3.9.1 ACTA2/vWF double staining

The 3 µm slides were put in the 37°C oven overnight and placed in the 58°C oven the next morning for one hour to melt the paraffine. The sections were deparaffinized in Xylol (3 x 10 min) and rehydrated in descending concentrations of ethanol (99,6% (twice), 96%, 70%, for 5 min each), followed by incubation with 3% H_2O_2-Methanol solution for 20 min to remove endogenous peroxidase. After washing with aqua dest. twice for 5 min, the slides were incubated with Proteinase K for 5 min at room temperature for epitope retrieval, then immersed in aqua dest. and washed with PBS pH 7,4 (4 x 5 min). Subsequently 10% Bovine serum albumin (BSA) was applied as a blocking buffer and

incubated for 20 min, followed by washing with PBS (4 x 5 min). Next, the slides were blocked for 30 min with Rodent Block M (Biocare Medical MM HRP-Polymer Kit, Cat. No. 1-800-799-9499), washed with PBS (4 x 5 min) and incubated with the primary antibody (Acta2 1:700 dilution, Fa. Sigma, Cat. No. A2547) for 30 min at room temperature. After washing with PBS (4 x 5 min) sections were incubated with HRP polymer for 20 min and washed again with PBS (4 x 5 min). As the next step the substrate solution was set up and applied (Vip substrate Kit, vector). The development of the staining was monitored under the microscope and when sufficient staining was completed the process was stopped after approximately 4 min by washing with deionized water and PBS for 5 min each.

The procedure of the vWF staining was opened by 20 min of blocking with 10% BSA, washing with PBS (4 x 5 min), followed by blocking with 2,5% normal horse serum (ImmPRESS Kit Anti-Rabbit Ig) for 20 min. The serum was decanted, and samples were incubated with the secondary antibody (vWF-antibody, 1:1000 dilution, Fa. Dako, Cat. No. A0082) for 30 min at 37°C and afterwards washed again with PBS (4 x 5 min). Then the sections were incubated for 30 min with Anti Rabbit Ig Peroxidase, washed with PBS (4 x 5 min) before the DAB substrate Kit (SK-4100, vector) was applied. Again, the samples were monitored under the microscope to decide when the ideal staining progression was reached (about 30 to 60 s depending on the tissue). The reaction was stopped by washing with deionized water for 5 min and counterstaining with methyl green for nuclei was performed on a heating plate (60°C) for one minute before washing with aqua dest. again. Finally, the sections were progressively dehydrated in ascending concentrations of ethanol, cleared in Xylol and covered with Pertex and glass.

3.9.2 ACTA2 staining for immunofluorescence

The 3 µm slides were deparaffinized in Xylol (3 x 7 min) and rehydrated in descending concentrations of ethanol (100%, 95%, 70%, 50% and 30%, for 2-3 min each). The sections were washed for 10 min in MilliQ H_2O at a stirrer. In the meanwhile, the rice cooker was turned on for following antigen retrieval and citrate buffer was preheated in the microwave for 2 min until boiling. The slides were then cooked in boiling citrate buffer in the rice cooker for 15 min and then let cool for 30 min submerged in ice until room temperature was reached. Next the slides were washed in PBS at a stirrer (3 x 5

min) before the blocking solution (3% BSA, 3% goat serum (GS)) was applied and incubated for 60 min at room temperature. After that, the incubation with the ACTA2-FITC antibody (SIGMA, Cat. No. F3777) (diluted with antibody solution (half concentrated blocking solution in PBS) 1:200) was performed over night at 4°C. On the second day the samples were washed in PBST at a stirrer (3 x 7 min) and in PBS (1 x 5 min). Prolong Gold antifade reagent with DAPI was applied to stain the nuclei and the stained slides were covered with glass.

3.10 Vascular morphometry

The previously for ACTA2 and vWF double stained 3 µm slides were used to measure the quantity of the pulmonary vessels and their degree of muscularization. The measurement was performed under the microscope at 40x magnification (20x or 10x for larger vessels) using the Leica Q Win Standard analyzing software for computer-assisted analysis. First the vessels were identified in the lung tissue by detection of the endothelial cells which stained positive for vWF and therefore appeared in a brown color. The vessels were selected manually and automatically classified by size according to the outer diameter calculated by the software (20-70 µm, 70-150 µm, >150 µm). In a second step the software detected the muscle cells around the vessels which stained positive for ACTA2 in a violet color. According to the degree of muscularization the vessels were divided into three groups: non-muscularized (no smooth muscle cell around the vessel), partially muscularized (up to 75% of the vessel surrounded by smooth muscle cells) and fully muscularized (more than 75% of the vessel surrounded by smooth muscle cells). This technique was applied to each slide, measuring all vessels.

3.11 Total surface measurement

To estimate the localization of the histological sample and to distinguish between proximal and distal parts of the lung for a better comparison in the groups, the total surface of each slide was measured using the Leica Q Win Standard analyzing software for computer-assisted analysis. In accordance with the macroscopic examination of the embedded lungs and the corresponding section plane the samples were divided into two groups. The samples with a total surface < 20 mm² were considered as sections from the more distal or peripheral area of the lung and the ones > 20 mm² from the proximal or

central area with a generally larger section plane. Figure 6 illustrates different section planes of the left lobe of the murine lung.

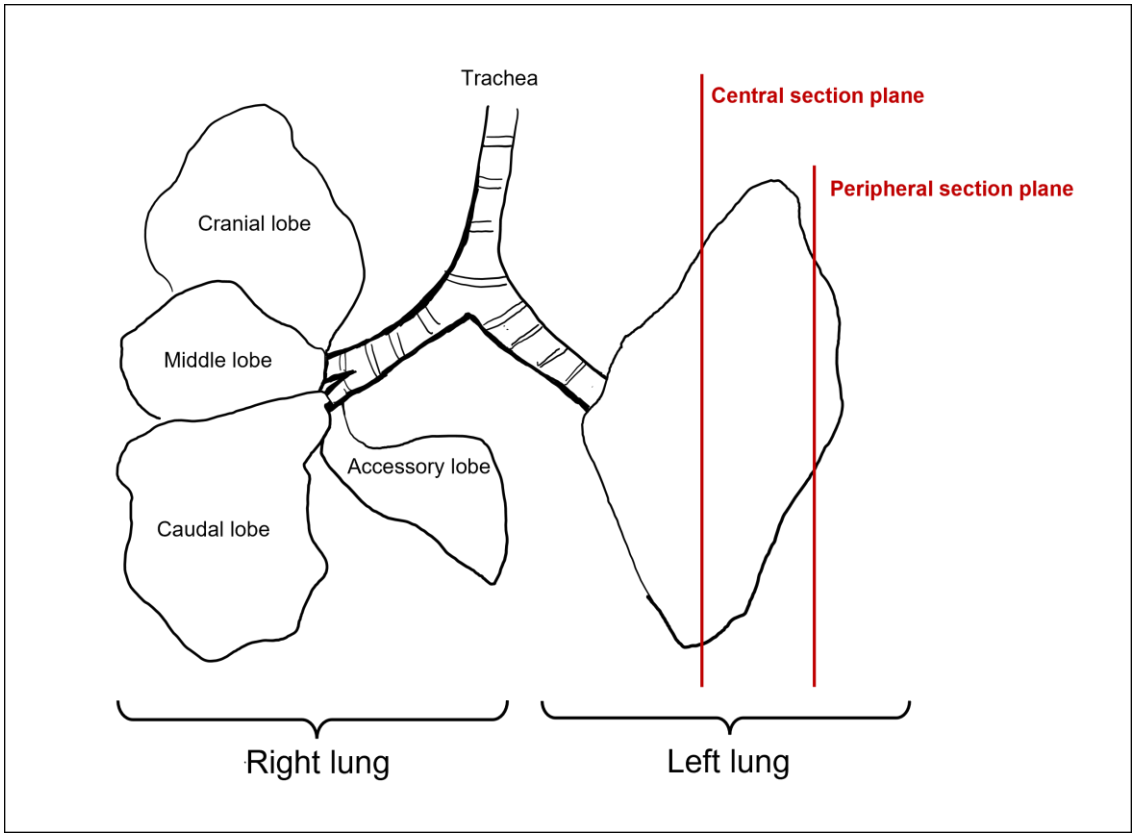

Figure 6: Scheme of the murine lung and illustration of different sectioning planes
The central section planes represent more proximal areas of the lung whereas the peripheral section planes cover mostly distal areas with alveoli and microvasculature.

3.12 Statistical analyses (Anova)

For all statistical analyses we used GraphPad PRISM statistical analysis software (GraphPad Software Inc., La Jolla, CA, USA). For each experimental group ROUT outliers` identification (for multiple outliers) and Grubb's alpha (for single outliers) were performed. To compare the three experimental groups one-way analysis of variance (ANOVA) tests were performed. P values <0.05 were considered as significant and presented as following: P values < 0.05: *; p values < 0.01: **; p values < 0.001: ***; p values <0.0001: ****. All data are presented as mean ± SD.

4 Results

4.1 Echocardiographic measurements indicate impaired function of the right ventricle in the hyperoxia PBS group and recovery under rFGF10 treatment

First, we intended to gain information about possible changes of the pulmonary blood pressure due to pathological remodeling of the lung vasculature. Therefore, echocardiography was performed on the mice before the lung harvest. We implemented this method in our experimental plan, since recent studies demonstrated the value of echocardiographic indices of right ventricular function for prediction of BPD (Neumann et al., 2021).

In the echocardiographic measurement several significant differences could be shown regarding the function of the right ventricle of the heart, which is strongly affected by changes in the pressure of the lung vasculature. The most important value is the TAPSE (tricuspid annular plane systolic excursion) which allows the estimation of the right ventricular function during the systolic cardiac action. The smaller the value of the TAPSE the weaker the function of the right ventricle. We found significantly decreased TAPSE values in the hyperoxia PBS group compared to the normoxia group (**Figure 7, A**).

This is a strong indication for impaired right ventricular function of the animals in this group which most likely results from pulmonary hypertension due to vascular remodeling, because the heart reacts directly to changes in the connected downstream vascular system. We did not find a significant difference between NOX and HYX FGF10. On the other hand, we observed a statistically significant increase of the TAPSE values in the HYX FGF10 group compared to the HYX PBS group (**Figure 7, A**). The body weight did not show significant differences between the groups, and the potential influence of weight on TAPSE measurements was excluded (**Figure 7, B**).

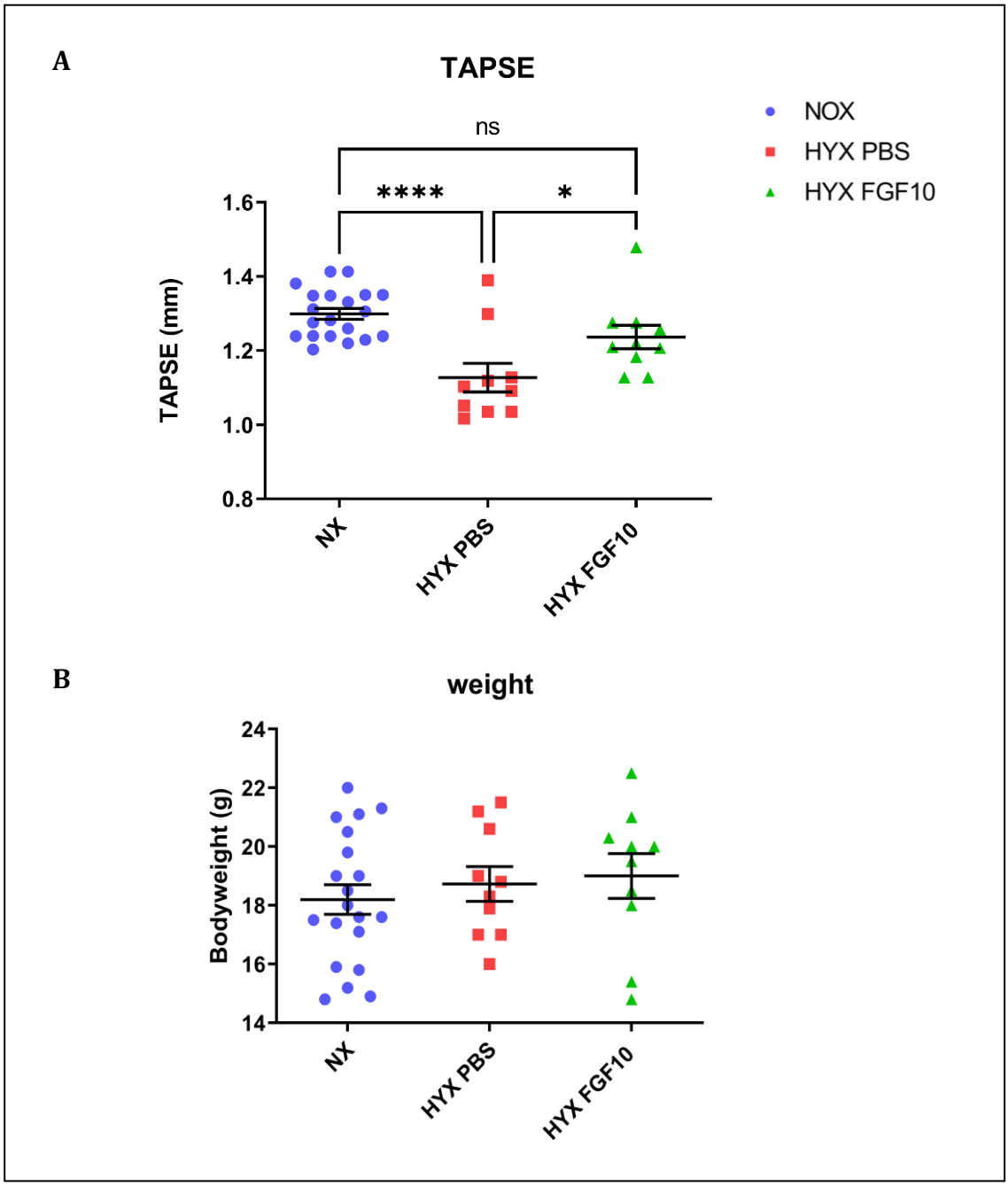

Figure 7: Echocardiographic measurements and weight of the mice at PN44

(A) TAPSE (tricuspid annular plane systolic excursion) measurement as an indicator for changes of the right ventricular function. The measurement shows a highly significant decrease of the TAPSE in the HYX PBS group. The HYX FGF10 mice showed significantly increased values and therefore improved right ventricular function.

(B) Weight measurement was supervised, and no significant difference was found.

P values < 0.05: *; p values < 0.01: **; p values < 0.001: ***; p values <0.0001: ****

Each dot represents one pup.

4.2 Lung function measurement shows different results for resistance (Rrs), compliance (Crs) and elastance (Ers) in the groups

Additionally, to the echocardiography, lung function was tested to study the mechanics of the lung directly. Therefore, we investigated three different parameters: compliance, elastance and resistance of the lungs.

The HYX FGF10 group showed a slightly higher compliance and therefore a higher ability of the lung to stretch passively compared to the other two groups (**Figure 8, A**). In line with this result the HYX PBS group reached higher values of elastance which acts as a reciprocal to the compliance and means that the stretchability of the lungs was decreased in this group (**Figure 8, B**).

Finally, we measured the resistance of the lung which describes how much resistance the air must overcome when passing the airways and acts reciprocal to the compliance. It mainly results from active flow resistance of the airways and friction during breathing and is determined by the balance between restoring force of the cartilage braces around the bronchial tubes and the surrounding lung tissue and the tone of the bronchial musculature. High resistance indicates that higher breathwork is required for inhalation. We found a similar trend for the resistance as for the elastance. The mice from the HYX PBS group showed an increased average value compared to the other groups, although the variability was high (**Figure 8, C**).

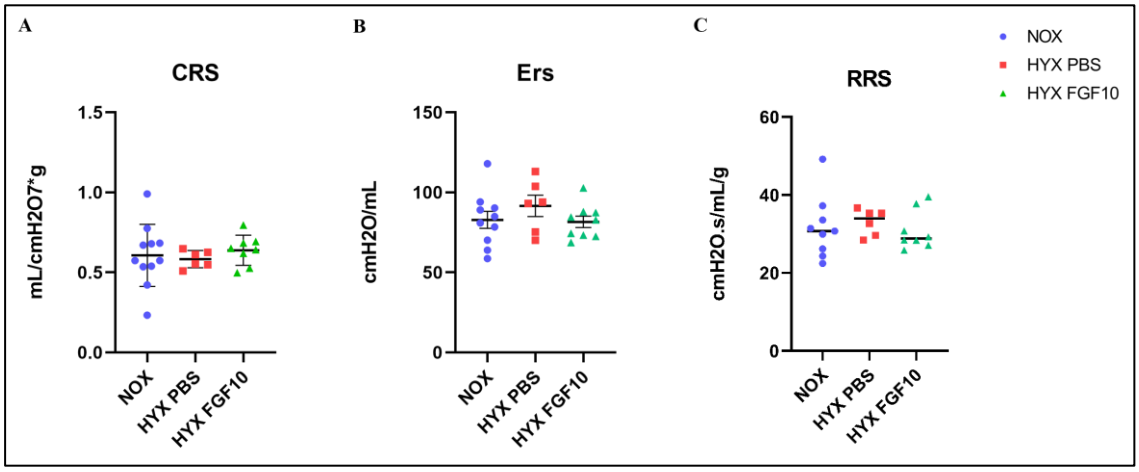

Figure 8: Lung function measurement at PN45

(A) The mice of the HYX FGF10 group showed a trend towards better compliance (CRS) which stands for higher stretchability of the lungs.

(B) The mice of the HYX PBS group showed increased elastance (Ers) and therefore decreased stretchability of the lungs.

(C) The resistance (RRS) shows a trend towards increased values after hyperoxic lung injury and a normalization after rFGF10 treatment.

P values < 0.05: *; p values < 0.01: **; p values < 0.001: ***; p values <0.0001: ****

Each dot represents one pup.

4.3 Mice show increased *Vegfa* and *Vegfr2/Kdr* expression after rFGF10 treatment

After finding several indications for changes of the pulmonary vasculature in the functional experiments we studied the expression of vascular markers by qPCR analysis after lung harvest.

Interestingly we determined changes of the expression of vascular endothelial growth factor (*Vegfa)*, which induces proliferation and migration of vascular endothelial cells. We found a downregulation of this factor after HYX lung injury compared to our control samples and on the other side an upregulation in the group treated with rFGF10 after hyperoxia close to statistical significance (**Figure 9a, A**).

Secondly, we found changes in the expression of vascular endothelial growth factor receptor 2/ kinase insert domain receptor (*Vegfr2/Kdr)* which binds on Vegfa and acts as an important regulator of angiogenesis and vasculogenesis. The expression of Vegfr2/Kdr was decreased in the Hyperoxia PBS group compared to control samples. The mice treated with rFGF10 showed an upregulated expression, which average was even higher than the control group (**Figure 9a, B**).

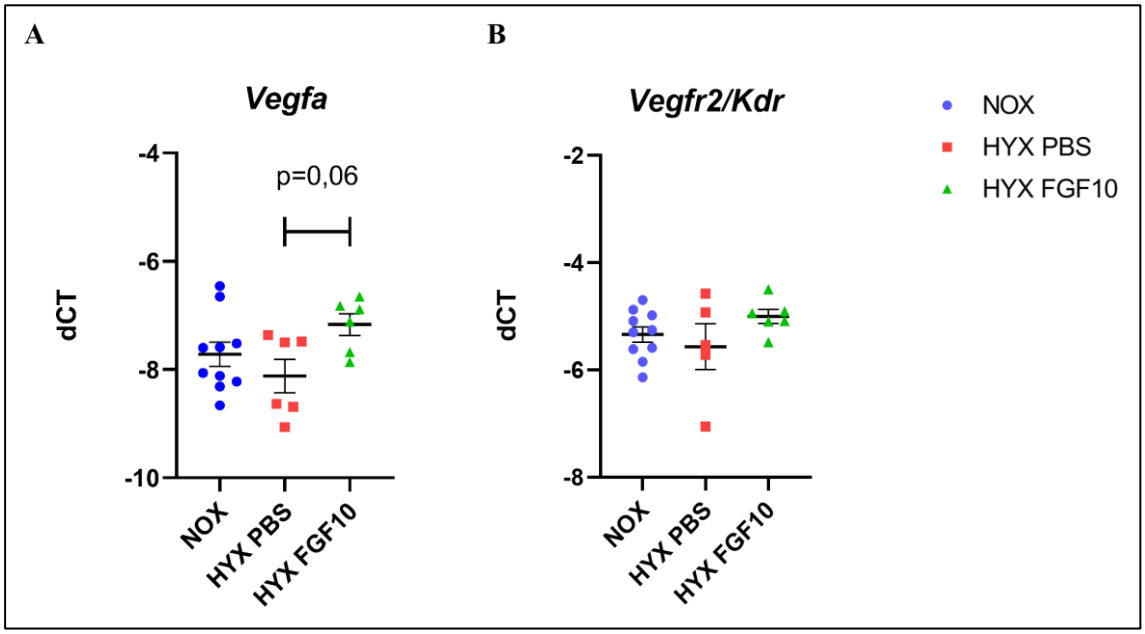

Figure 9a: Expression of genes connected to the development of the pulmonary vasculature *Vegfa:* vascular endothelial growth factor, *Vegfr2/Kdr:* vascular endothelial growth factor receptor/ kinase insert domain receptor, dCT: delta cycle threshold (GAPDH – TARGET).

(A) qPCR for *Vegfa* in mouse lungs from PN45. Mice of the HYX PBS group showed decreased levels of *Vegfa* mRNA expression whereas lungs after rFGF10 treatment displayed increased levels.

(B) qPCR for *Vegfr2/Kdr* in mouse lungs from PN45. The *Vegfr2/Kdr* mRNA expression was decreased in the HYX PBS group and increased in the HYX FGF10 group.

P values < 0.05: *; p values < 0.01: **; p values < 0.001: ***; p values <0.0001: ****

Each dot represents one pup.

4.4 Increased levels of *Fgf7* and other genes suggest enhanced regeneration of lung tissue

Apart from the just described vascular markers we examined additional genes that are associated with regeneration processes and detected several statistically significant changes in further qPCR measurements.

First, we found a strong upregulation of *Fgf7* in the HYX PBS group as well as in the HYX FGF10 group. FGF7 and FGF10 both bind to the receptor FGFR2b. Furthermore, we were able to demonstrate a statistically significant upregulation of *Cldn1* in the HYX FGF10 group, a marker of intercellular barrier function. The difference between the NOX and HYXPBS group was not statistical.

Finally, we studied the level of platelet endothelial cell adhesion molecule (*Pecam1*), also known as cluster of differentiation 31 (*Cd31*), which is mainly found on endothelial cells. We demonstrated a significant upregulation of *Pecam1* in the HYX FGF10 group compared to our control (**Figure 9b**).

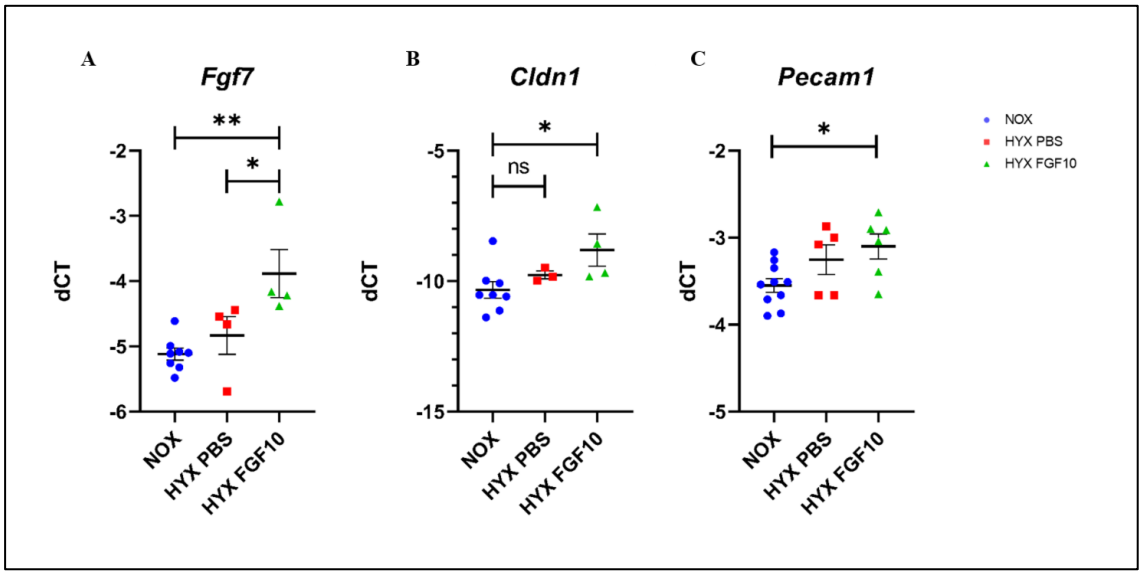

Figure 9b: Expression of genes associated with regeneration after injury of inflammation and endothelial proliferation

Fgf7: Fibroblast growth factor 7; *Cldn1:* Claudin 1; *Pecam1:* platelet endothelial cell adhesion molecule 1.

(A) qPCR for *Fgf7* in mouse lungs from PN45. Samples from the HYX FGF10 group showed highly significant increased levels of *Fgf7* mRNA compared to the NOX group and a statistical difference compared to the HYX PBS group.

(B) qPCR for *Cldn1* in mouse lungs from PN45. mRNA levels of HYX FGF10 lungs were significantly increased.

(C) qPCR for *Pecam1* in mouse lungs from PN45. Again, we were able to demonstrate a significant increase of mRNA levels in the HYX FGF10 group compared to NOX.

P values < 0.05: *; p values < 0.01: **; p values < 0.001: ***; p values <0.0001: ****

Each dot represents one pup.

4.5 Vascular morphometry (ACTA2/vWF double staining) reveals decreased number of vessels mainly in the distal areas of the lung

After we collected data about the function of the murine heart and lung in vivo in our BPD model, as well as the expression of vascular markers in qPCR analysis, we were specifically interested in the histological features and therefore studied the pulmonary vasculature at PN45 by the ACTA2/vWF double staining (**Figure 10**) followed by vascular morphometry.

This method allowed us to quantify the number of vessels and the extent of muscularization. Based on their diameter and degree of muscularization, pulmonary vessels were categorized into three size groups (20-70 µm, 70-150 µm and >150µm) and three muscularization groups (fully, partially and non-muscularized). Furthermore, the overall surface of all previously cut and stained slides was measured, and the samples were divided into two groups according to their surface to ensure comparability of the results: one smaller than 20 mm^2 and one larger than 20 mm^2. This classification corresponds, on the one hand, to the more distal, peripherally sectioned regions of the lungs, which contain most of the microvasculature, and on the other hand, to the proximal, central regions.

In the quantification of the vascular morphometry of the samples smaller than 20 mm^2 we found a significantly decreased total number of vessels in the HYX PBS group compared to the NOX group. This rarefication of pulmonary vasculature in the distal areas of the lung was less severe in the HYX FGF10 group. Compared to the HYX PBS group the animals treated with rFGF10 showed an increased total number of vessels and a tendency back to the NOX group (**Figure 11, C**). In the samples with a surface larger than 20 mm^2 the HYX PBS group showed an increased number of vessels while the number decreased slightly after rFGF10 treatment (**Figure 11, D**). The results show a wide range but are equally distributed between the groups.

The rarefication of vessels we found in the HYX PBS group was supported by the results of the vessels´ density measurement. We calculated the number of vessels per mm^2 and found a decreased density of vessels in the HYX PBS samples compared to NOX <20 mm^2 (**Figure 11, A**).

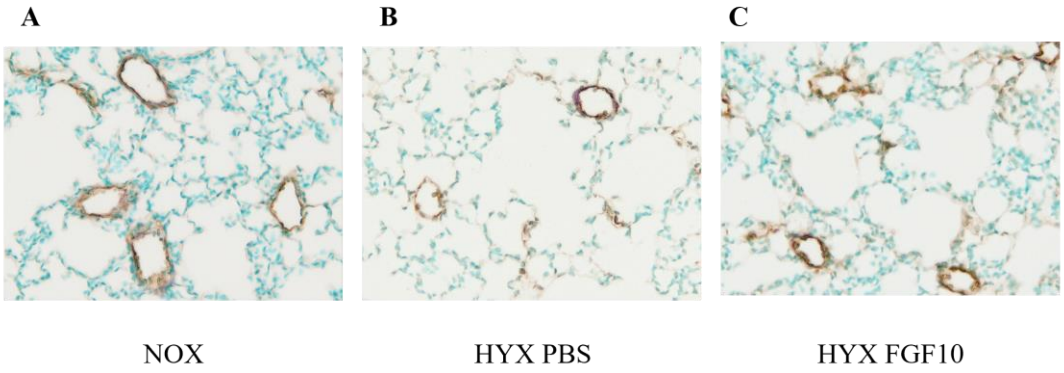

Figure 10: Representative histological ACTA2 / vWF double staining of murine lung tissue

ACTA2 / vWF double staining of lung sections from NOX, HYX PBS and HYX FGF10 mice at postnatal day 45. vWF-positive cells appear in a brown color; ACTA2-positive cells are stained purple which appears generally darker in the samples. All nuclei of the cells are stained in a light blue.

All pictures were taken from samples with a surface < 20 mm², representing distal areas of the lungs. Pictures were captured at 40x magnification.

(A) NOX: Normoxia; (B) HYX PBS: Hyperoxia PBS; (C) HYX FGF10: Hyperoxia FGF10.

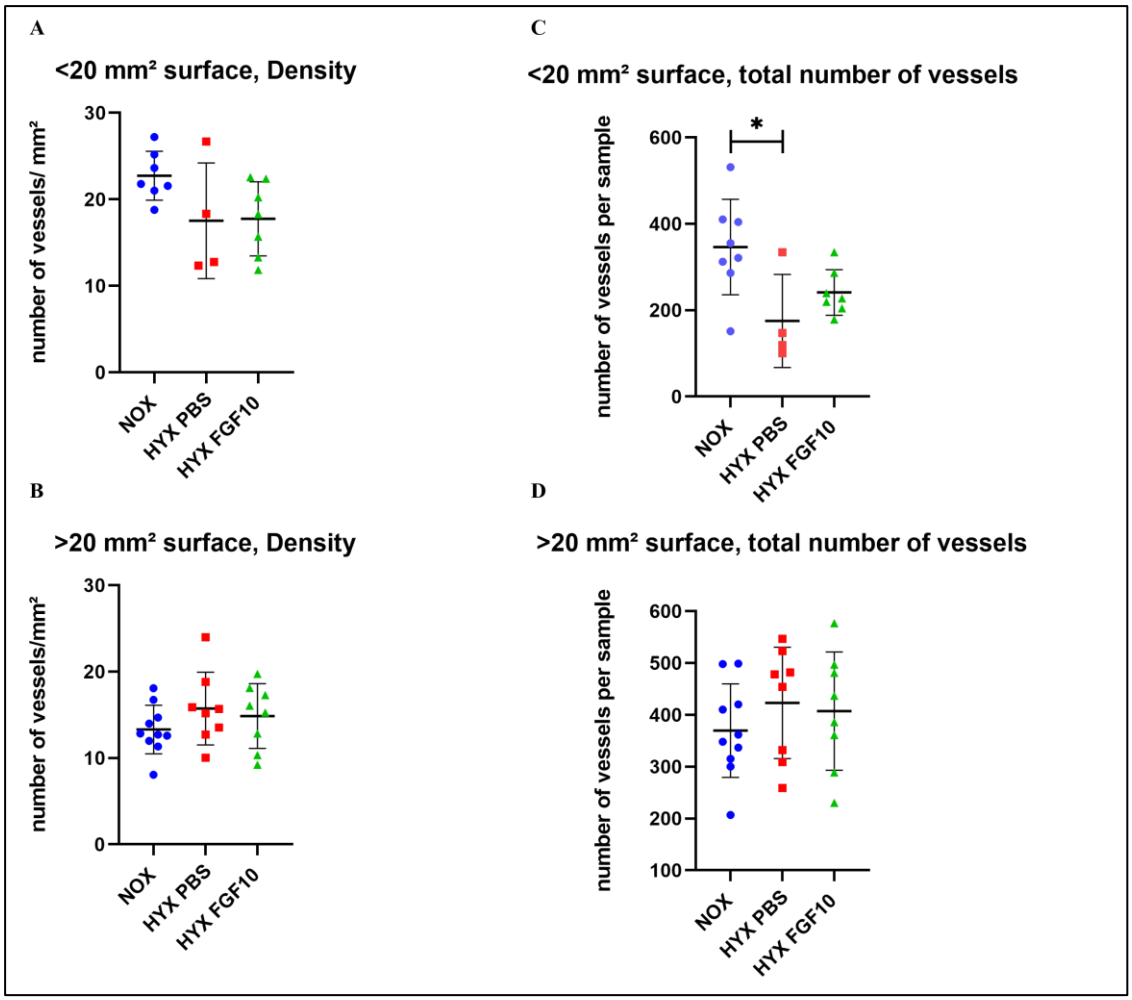

Figure 11: Vascular morphometry measurement, total number of vessels and density of vessels in the lung

(A) Density of vessels in samples with a surface < 20 mm²: We found decreased vessel density in the HYX groups.

(B) Density of vessels in samples with a surface >20 mm²: In this group we found slightly increased vessel density in the HYX OBS samples.

(C) Results of the samples with a surface <20 mm² (distal areas of the lung): HYX PBS lungs showed a decrease of vessels in the distal areas of the lung. This rarefication of vessels normalized under rFGF10 treatment.

(D) Results of the samples with a surface >20 mm² (central areas of the lung): In the samples which represented mostly central areas of the lung the trend of the rarefication of vessels was reversed with an increased number of vessels in the HYX PBS group.

P values < 0.05: *; p values < 0.01: **; p values < 0.001: ***; p values <0.0001: ****
Each dot represents one pup.

4.6 Increased percentage of fully muscularized small vessels after HYX lung injury and normalization after rFGF10 treatment

Furthermore, we measured the percentage of fully, partially and non-muscularized vessels to describe distribution of muscularization in our samples.

In the category of small vessels (20-70 μm) in the samples smaller than 20 mm² the percentage of fully muscularized vessels was increased in the HYX PBS group compared to mice held under NOX conditions. In the HYX FGF10 group we counted less fully muscularized vessels and the average of this group was close to our control samples (**Figure 12, A**). In the group of samples with a surface >20 mm² we saw the opposite trend, with less fully muscularized vessels in the HYX PBS group compared to the other two experimental groups (**Figure 12, B**).

Next, we measured the percentage of partially muscularized vessels with a diameter from 20 to 70 μm. Interestingly in this case the HYX PBS group showed a decreased percentage of partially muscularized vessels compared to NOX and HYX FGF10. Due to high variability in the groups, we did not reach statistical significance in this measurement (**Figure 12, C and D**).

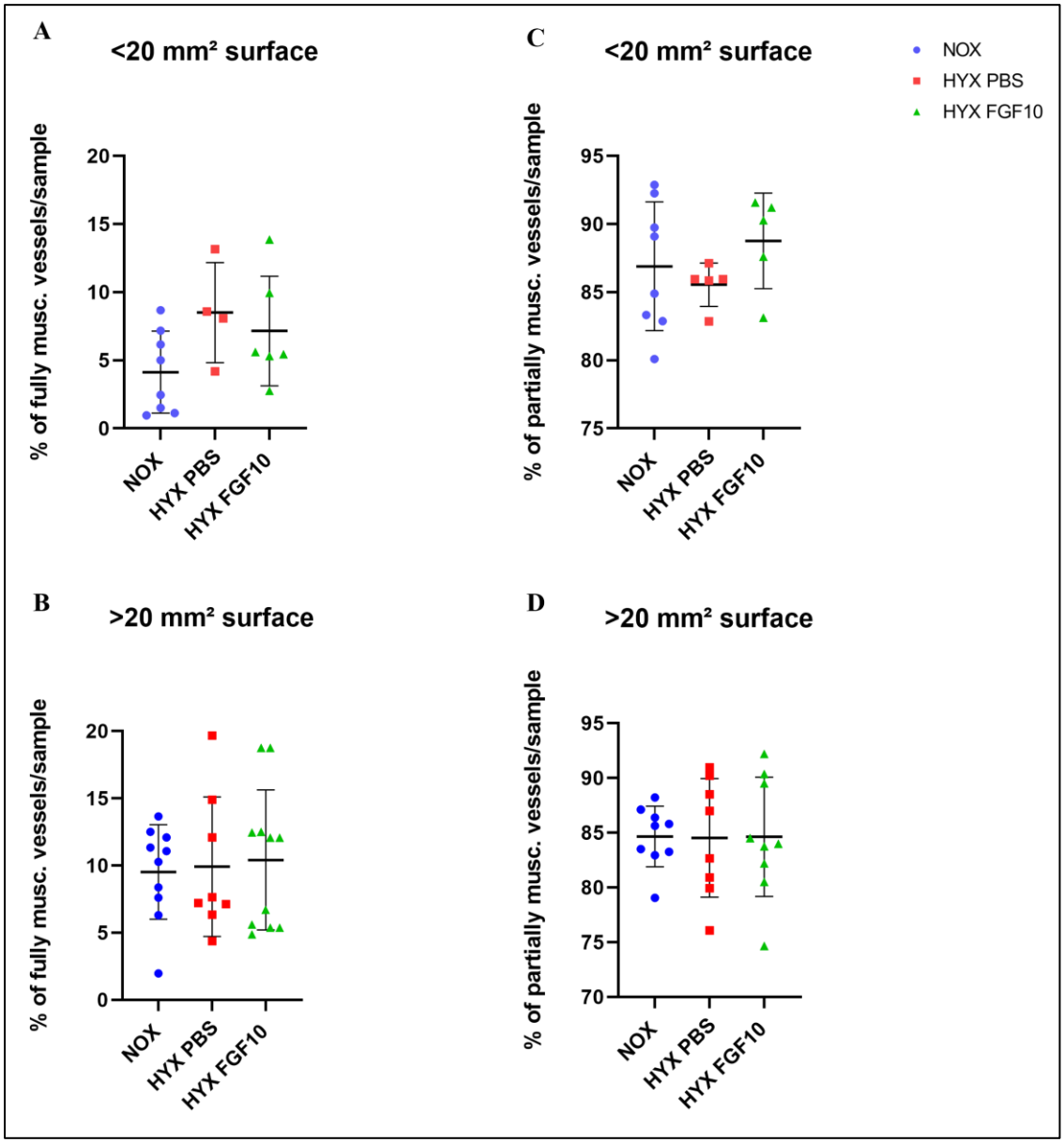

Figure 12: Vascular morphometry, percentage of fully and partially muscularized vessels with a diameter from 20 to 70 µm

(A) Samples with a surface <20 mm² showed an increased percentage of fully muscularized vessels in the HYX PBS group

(B) In samples from the central areas of the lung with a surface >20 mm² the percentage of fully muscularized vessels was not changed.

(C) In samples with a surface < 20mm² the percentage of partially muscularized was increased in the HYX FGF10 group and slightly decreased in the HYX PBS group.

(D) In the group with a surface > 20 mm² we did not see a difference.

Each dot represents one pup.

4.7 ACTA2 immunofluorescence does not reveal evidence of aberrant structural remodeling

To investigate whether rFGF10 treatment leads to abnormal structural remodeling of the lung tissue, we performed immunofluorescence staining for α-smooth muscle actin (ACTA2) on sections collected at postnatal day 45. ACTA2 is expressed by vascular smooth muscle cells and interstitial myofibroblasts and is commonly used to assess smooth muscle architecture in pulmonary tissue.

Across all groups, ACTA2-positive structures displayed a distribution consistent with normal vascular anatomy. We did not detect focal accumulations, disorganized clusters, or architectural anomalies indicative of excessive or aberrant remodeling. Morphologically, the samples retained preserved alveolar and vascular compartmentalization (**Figure 13**).

However, ACTA2 alone does not capture broader aspects of structural remodeling, such as changes in extracellular matrix composition or alterations in cellular proliferation and differentiation. Therefore, while no overt anomalies were observed, these findings are descriptive and should be interpreted cautiously. A comprehensive assessment of tissue remodeling would require additional analyses, including matrix visualization, quantification of proliferative markers, and molecular profiling.

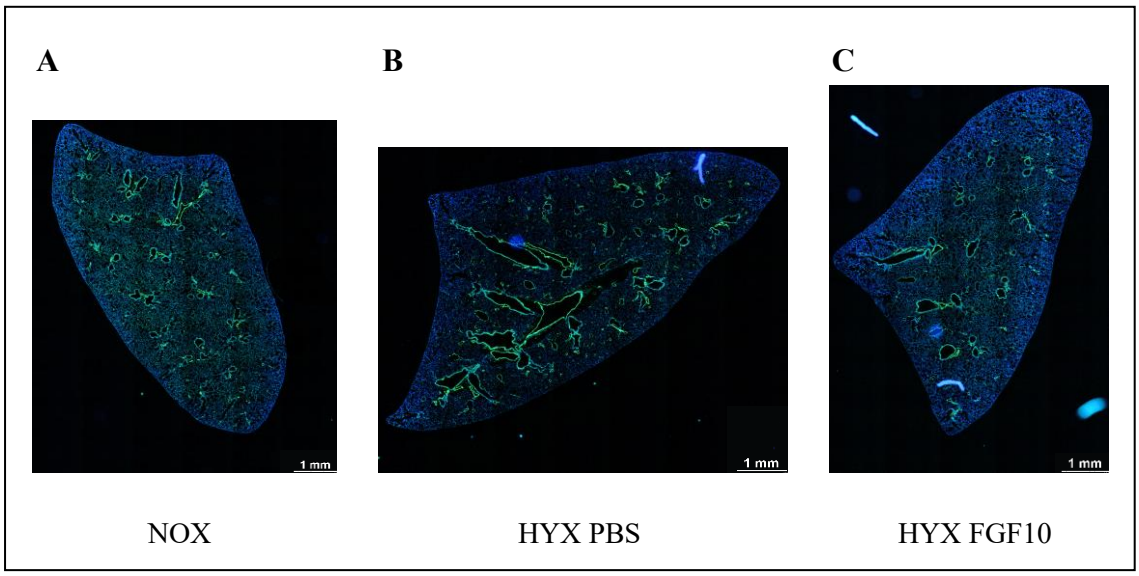

Figure 13: Tilescan immunofluorescence of murine lung tissue

Representative confocal tilescan image of postnatal day 45 lung sections from NOX, HYX PBS and HYX FGF10 mice.
Staining shows ACTA2-positive cells (green) and nuclei (DAPI, blue).
Scale bar: 1 mm.

(A) NOX: Normoxia; (B) HYX PBS: Hyperoxia PBS; (C) HYX FGF10: Hyperoxia FGF10

5 Discussion

Our study investigated, for the first time, the connection of hyperoxia induced lung injury and the vascular system of the lung, as well as the impact of rFGF10 treatment in a mouse model of BPD at a particularly late timepoint of lung maturation. Our findings confirm the clear involvement of the vascular system in the pathogenesis of chronic lung disease in this mouse model of BPD. The experimental group treated with rFGF10 exhibited improved lung function and significantly enhanced right ventricular function in echocardiographic measurements compared to the control group. Vascular morphometry revealed a rarefication of pulmonary vessels and an increase in fully muscularized vessels in the experimental group exposed to hyperoxia and treated with PBS. Our histological experiments under rFGF10 treatment strongly suggest enhanced recovery of the pulmonary vasculature, supported by our qPCR measurements showing increased expression of *Vegfa* and its receptor *Vegfr2/Kdr*.

Overall, our results underscore the pivotal role of the pulmonary vascular system in the development and prognosis of BPD. We found compelling evidence pointing to the strong potential of rFGF10 treatment in promoting the regeneration of pulmonary vasculature in our model, offering a promising therapeutic avenue for BPD patients.

5.1 Clear effect of hyperoxia on the pulmonary vasculature in a mouse model of bronchopulmonary dysplasia

The existing body of research has already demonstrated the impact of hyperoxia on the airways. Our experiments aim to shed light on its effects on the vasculature, which are not yet fully understood. We have observed significant impacts not only on the bronchial system but also on the pulmonary vessel tree. This supports the hypothesis that BPD has a notable vascular component, as confirmed by our functional measurements of lung and heart. Our findings indicate impaired organ function, decreased vascular endothelial growth factors, and clear histological changes indicative of a PH-phenotype, as observed in the vascular morphometry. These findings align with the impaired right ventricular function identified in the echocardiography.

Additionally, we noted a substantial upregulation of *Fgf7* expression in both HYX groups, possibly in response to tissue injury following exposure to hyperoxia. Notably,

the HYX FGF10 group exhibited the highest expression of *Fgf7*, suggesting a more robust regeneration process following treatment with rFGF10, in which FGF7 is involved and consequently upregulated in this group. Given that both FGF7 and FGF10 are ligands of FGFR2b, we speculate a positive feedback mechanism exists between increased levels of Fgf10, possibly acting as an autocrine signal, and increased levels of Fgf7. It is also plausible that feedback mechanisms between different cell types, such as from epithelial to mesenchymal cells, contribute to the upregulation of Fgf7 following rFGF10 treatment.

All our methods consistently revealed the effects of hyperoxia in the experimental group treated with PBS compared to the NOX group, providing evidence of BPD-associated damage to the pulmonary vasculature in our model.

5.2 Improvement of lung function, right ventricular function, and histological features after rFGF10 treatment

According to previous studies, we assume a downregulation of *Fgf10* after exposure to hyperoxia in the HYX PBS group. We aimed to restore these levels with rFGF10 treatment as a replacement therapy in the HYX FGF10 group. All experiments showed a trend toward normalizing measurement results after the rFGF10 treatment. This indicates positive effects of our treatment with rFGF10 and suggests potential contributions of FGF10 to pulmonary recovery mechanisms after lung damage in BPD, particularly those targeting the vascular system.

Echocardiography results revealed highly significant differences between the groups. The significantly decreased TAPSE values in the HYX PBS group compared to the NOX group indicate impaired right ventricular function, likely due to increased pulmonary pressure from vascular remodeling in the lung. In contrast, the HYX FGF10 group showed a significant increase in TAPSE values compared to the PBS group, suggesting a highly improved right ventricular function. This indicates that vascular remodeling after hyperoxia, which lead to impaired right ventricular function, was partially reversed after rFGF10 treatment. There was no statistically significant difference between the TAPSE values of the NOX and HYX FGF10 group, which supports our theory.

High TAPSE values indicate higher pulmonary pressure, leading to a higher load on the right ventricle. Increased pulmonary pressure can result from an increased degree of

muscularization of the pulmonary vasculature. In support of this idea, we found a higher number of fully muscularized small vessels in the distal areas of the lungs from the HYX PBS group. Additionally, a high number of collapsed vessels might also contribute to the increased pressure. Although the results of lung function were not statistically significant, all measurements showed a clear trend in the same direction: impaired lung function after BPD-like damage of the lung and improvement in the group treated with rFGF10. The hyperoxia PBS group showed higher values for elastance and resistance, indicating decreased stretchability of the lungs, which required increased breathwork for inhalation. Although lung function measurements allow only indirect conclusions about the pulmonary vasculature, they provide information about the phenotype and symptoms of the experimental animals.

Histological studies based on the ACTA2/vWF double staining revealed a rarefication of vessels in the distal areas of the lung and an increased percentage of fully muscularized small vessels. We first stained the samples for endothelial cells to identify the vessels in the pulmonary tissue and then stained the smooth muscle cells to estimate the degree of muscularization of the counted vessels in the following vascular morphometry. This method allowed us to focus on the overall number of vessels and to discover a rarefication of vessels in the experimental group treated with PBS. Furthermore, we demonstrated an increase in fully muscularized small vessels, which might explain the impaired function of the right ventricle of the heart in this group, similar to mice suffering from pulmonary hypertension. The mice treated with rFGF10 after exposure to hyperoxia showed improved results: a higher total vessel count and fewer fully muscularized small vessels. The effect of rFGF10 treatment may be even stronger at an earlier timepoint when the initial damage takes place.

5.3 Stronger effects on distal areas of the lung

We observed different results depending on the plane of the lung where the slice was cut. Based on the position during the cutting process, we classified samples with a surface larger than 20 mm² as proximal areas of the lung and samples with a surface smaller than 20 mm² as distal areas of the lung. In our histological experiments the distal parts were more severely affected by hyperoxia and showed a stronger reaction to our treatment with rFGF10. One possible explanation for this phenomenon could be that the alveolo-

capillary barrier is thinner in the distal and peripheral areas of the lung. As a result, distal vessels might be more affected by oxygen toxicity from the inhaled air which directly affects the surrounding tissue closest to the airways. Due to the proximity of the different cells in this area, the epithelial-endothelial crosstalk is likely more intense, allowing a stronger reaction to rFGF10 treatment and higher potential for regeneration. Also, the distal airways and vessels develop later than the proximal ones and therefore might be more affected by hyperoxia and the rFGF10 treatment because the cells are still in a process of division and are more susceptible to external influences. Another explanation could be that the origin of the proximal and distal cells might be different, so they react differently to the treatment. Further research is needed to identify whether the observed effects on the pulmonary vasculature are directly related to FGF10 or indirect transmission through mediators. Although many targets and feedback loops of FGF10 are well studied, the role of the vasculature in this system is not yet fully understood.

5.4 Limitations of this study

The findings of the current investigation offer valuable insights into the regional responses of the murine lung to hyperoxia and the administration of rFGF10. Despite several notable strengths, it is important to acknowledge certain limitations when interpreting the results of this study.

Firstly, the study is subject to high variability in results due to inherent sample variability. Individual mice exhibit diverse reactions to the treatment, necessitating a sizable number of animals to achieve statistical significance while simultaneously minimizing the use of laboratory animals for ethical reasons. Consequently, statistical significance may not be attained due to interexperimental variability. Nevertheless, it is worth noting that operator and technical variability are minimal, as each experiment was conducted by a single operator using consistent techniques and protocols. Thus, while the results are reliable, enhancing the sample size in future studies could further bolster their robustness.

Secondly, the analysis software employed for vascular morphometry does not account for vessels with a diameter smaller than 20 µm, potentially resulting in the loss of information pertaining to the smallest capillaries and microvasculature. Small vessels are particularly susceptible to damage and essential for effective gas exchange in the lungs. Given that our findings indicate a significant impact of our treatment on small vessels, capturing

vessels smaller than 20 µm could provide a more comprehensive understanding of this effect.

Additionally, the harvesting process led to the collapse of numerous vessels, likely attributed to the established flushing method or the rFGF10 treatment. The diameter of these collapsed vessels could not be estimated and had to be excluded from the analysis, posing a challenge to the accuracy of our results.

Furthermore, limitations associated with the cutting of embedded blocks resulted in imperfectly cut vessels, impeding the precise measurement of each vessel's real diameter. This inherent variability may yield partially inaccurate results in histological studies. However, given that this issue is consistent across all samples, the deviation from actual values does not disproportionately impact specific groups, thereby allowing the results to be utilized.

5.5 Importance of this study for clinical setting

Due to our late timepoint of lung harvest, we were able to observe the long-term effects of BPD-related lung damage, focusing specifically on the vascular system. This study holds clinical significance due to its extended duration and emphasis on the vascular component, a facet that, to our knowledge, has not been previously documented in literature. The findings provide insight into the impact of hyperoxia and rFGF10 treatment in conjunction with natural regenerative processes over time. Managing BPD in the long term remains a significant challenge for healthcare professionals, underscoring the need for more information on potential treatments.

While it's important to note that these results from an animal model cannot be directly applied to human patients, the substantial functional improvements observed in echocardiography as a result of rFGF10 treatment are indicative of its strong impact on organ function, a critical factor for the physical well-being and quality of life of BPD patients, particularly in adulthood. Although some histological damage may be permanent and irreversible, influencing the symptoms of the affected cardio-pulmonary system could significantly enhance everyday clinical practice.

5.6 Future perspectives

This study presents significant findings on the role of the vascular network in the development of BPD and its influence on associated comorbidities, including BPD-PH and PVD. The results indicate that rFGF10 treatment has a positive impact on the pulmonary vasculature, leading to notable improvements in heart and lung function. These changes were observed in mice at PN45, suggesting that vascular injuries play a critical role in the long-term consequences of BPD.

Future studies should consider investigating earlier timepoints and different stages of development to gain a better understanding of the extent of damage and repair mechanisms over time. Additionally, exploring the origins of cells and potential crosstalk in different lung regions will provide valuable insights into regional variations and the potential for regeneration. Investigating whether the number of collapsed vessels differs between the NOX and HYX groups and exploring possible causative correlations would be beneficial. Furthermore, utilizing methods such as X-ray microtomography (microCT) to measure the microvasculature more precisely will contribute to the comprehensive understanding of this intricate network.

6 Summary

There is strong evidence for the essential role of FGF10 during lung development. However, little is known about its concrete effect on the vascular system and the contribution of pulmonary vasculature to the pathogenesis of BPD. We aimed to study the impact of rFGF10 on the vasculature of the lung in a mouse model of BPD, to gain new information about underlying mechanisms and related pathologies such as BPD-PH. To demonstrate the effect of hyperoxia-induced lung injury, we exposed two experimental groups to hyperoxia (HYX) (PN1-PN8) followed by several intraperitoneal injections of PBS or rFGF10 until PN42. In the following experiments, we compared these groups to a control group held under normoxic conditions (NOX). Before lung harvest on PN45, we performed lung function and echocardiographic measurements to study organ function indices. We found strong indications for impaired right ventricular function represented by high TAPSE values in the HYX PBS group, suggesting an increased pressure of the pulmonary vascular system connected downstream of the right ventricle of the heart. The HYX FGF10 group showed a normalization of all studied indices in the functional experiments. Afterward, we collected lungs for further analysis involving RT-qPCR, immunostainings, and vascular morphometry after a double staining with ACTA2 and vWF. In summary, we found increased expression of *Vegfa* and its receptor *Vegfr2* in the qPCR after rFGF10 treatment. The vascular morphometry revealed a rarefication of vessels in the distal areas of the lung after exposure to hyperoxia and regeneration after rFGF10 treatment. Furthermore, we were able to demonstrate an increased percentage of fully muscularized vessels towards a PH-phenotype after HYX lung injury and normalization after rFGF10 treatment in the periphery of the lung. Our results provide evidence for the affection of the pulmonary vasculature in a mouse model of BPD and the beneficial effects of rFGF10 treatment at a late stage of lung development. We found improved organ function, upregulated expression of pro-angiogenic genes and normalized histological features in the HYX FGF10 group compared to the HYX PBS group. In conclusion, this study reveals important information about changes of the pulmonary vasculature after hyperoxic lung injury at PN45, which represents young adulthood of the mice. We were able to partly reverse the damage described with our rFGF10 treatment. These findings might be crucial in developing targeted therapies to prevent or treat BPD and associated vascular comorbidities in prematurely born infants.

7 Zusammenfassung

Die wesentliche Rolle von FGF10 für die Entwicklung der Lunge ist hinreichend belegt. Allerdings ist wenig über konkrete Effekte auf das Blutgefäßsystem der Lunge und dessen Beitrag zur Pathogenese von BPD bekannt. Um neue Informationen über zugrundeliegende Mechanismen und verwandte Pathologien, wie BPD-PH, zu erlangen, untersuchten wir die Wirkung von rFGF10 auf die pulmonalen Gefäße in einem Maus-Modell für BPD. Wir demonstrierten den Effekt von Hyperoxie-induzierter Lungenschädigung, indem wir die Experimentalgruppen Hyperoxie (HYX) aussetzten, gefolgt von mehreren intraperitonealen Injektionen von PBS oder rFGF10. In den anschließenden Experimenten verglichen wir diese Gruppen mit einer Kontrollgruppe, die unter normoxischen Bedingungen (NOX) gehalten wurde. Vor der Lungenentfernung an PN45 führten wir zur Untersuchung der Organfunktion eine Lungenfunktionsmessung und Echokardiographie durch. Wir fanden deutliche Zeichen einer eingeschränkten rechtsventrikulären Funktion, repräsentiert durch hohe TAPSE-Werte in der HYX PBS Gruppe. Dies legt einen erhöhten Druck im pulmonalen Gefäßsystems nahe. Die HYX FGF10 Gruppe zeigte eine Normalisierung der Werte in allen funktionellen Experimenten. Anschließend verwendeten wir die Lungen für weitere Analysen, darunter RT-qPCR, Immunfärbungen und vaskuläre Morphometrie nach Doppelfärbung mit ACTA2 und vWF. Wir fanden gesteigerte Expression von *Vegfa* und *Vegfr2* in der HYX FGF10 Gruppe. Die vaskuläre Morphometrie enthüllte eine Gefäßrarefizierung in distalen Lungenarealen nach HYX sowie eine Regeneration nach rFGF10 Behandlung. Außerdem konnten wir einen erhöhten Anteil voll muskularisierter Gefäße nach HYX feststellen, ähnlich eines PH-Phänotypen, sowie eine Normalisierung der Werte in der HYX FGF10 Gruppe. Die Ergebnisse weisen auf eine Schädigung pulmonaler Gefäße in unserem BPD-Mausmodell und Regeneration nach rFGF10 Behandlung hin. Wir stellten in der HYX FGF10 Gruppe verglichen mit der HYX PBS Gruppe verbesserte Organfunktion, gesteigerte Expression pro-angiogenetischer Gene und normalisierte histologische Merkmale fest. Zusammenfassend liefert die Studie wichtige Informationen über Veränderungen der pulmonalen Gefäße nach hyperoxischer Lungenschädigung an PN45, was einem frühen Erwachsenenalter der Mäuse entspricht. Die beobachteten Schäden waren nach rFGF10 Behandlung teilweise reversibel. Diese Erkenntnisse könnten somit zur Entwicklung gezielter Therapien zur Prävention oder Behandlung von BPD und assoziierten vaskulären Komorbiditäten bei Frühgeborenen beitragen.

8 Abbreviations and Acronyms

ACTA2	Actin alpha 2
AT2	Alveolar type 2
BMP4	Bone morphogenetic protein 4
BPD	Bronchopulmonary dysplasia
BPD-PH	Bronchopulmonary associated pulmonary hypertension
BSA	Bovine serum albumin
Cldn1	Claudin1
Crs	Compliance
DA	Ductus arteriosus
DAPI	4′,6-diamidino-2-phenylindole
E	Embryonic
Echo	Echocardiography
ECM	Extracellular matrix
Ers	Elastance
FGF	Fibroblast growth factor
FGFR	Fibroblast growth factor receptor
GA	Gestational age
HIF	Hypoxia-inducible factors
HRP	Horseradish peroxidase
HSPG	Heparan Sulfate ProteoGlycan
HYX	Hyperoxia

iNO	Inhaled nitric oxide
IP	Intraperitoneal
IUGR	Intrauterine growth retardation
IL	Interleukin
Kdr	Kinase insert domain receptor
mTORCH1	Mammalian target of rapamycin complex 1
NOX	Normoxia
PH	Pulmonary hypertension
PIH	Pregnancy induced hypertension
PMA	Postmenstrual age
PN	Postnatal
PVD	Pulmonary vascular disease
PBS	Phosphate-buffered saline
PBST	Phosphate-buffered saline with tween
Pecam1	Platelet endothelial cell adhesion molecule 1
PFA	Paraformaldehyde
rFGF10	Recombinant fibroblast growth factor 10
RNA	Ribonucleic acid
ROS	Reactive oxidant species
Rrs	Resistance
RVID	Right ventricular internal diameter

RVWT	Right ventricular wall thickness
SHH	Sonic hedgehog
TAPSE	Tricuspid annual plane systolic excursion
TGF-ß	Transforming growth factor beta
TLR	Toll-like receptor
TNF	Tumor necrosis factor
Vegfa	Vascular endothelial growth factor
Vegfr2	Vascular endothelial growth factor receptor
VILI	Ventilation induced lung injury
VSMCs	Vascular smooth muscle cells
vWF	von Willebrand Factor

9 List of tables and figures

Tables

Figures

10 References

Abman, S. H., Bancalari, E., & Jobe, A. (2017). The Evolution of Bronchopulmonary Dysplasia after 50 Years. *American journal of respiratory and critical care medicine*, *195*(4), 421–424. https://doi.org/10.1164/rccm.201611-2386ED

Arjaans, S., Zwart, E. A. H., Ploegstra, M. J., Bos, A. F., Kooi, E. M. W., Hillege, H. L., & Berger, R. M. F. (2018). Identification of gaps in the current knowledge on pulmonary hypertension in extremely preterm infants: A systematic review and meta-analysis. In *Paediatric and Perinatal Epidemiology* (Vol. 32, Issue 3, pp. 258–267). Blackwell Publishing Ltd. https://doi.org/10.1111/ppe.12444

Benjamin, J. T., Smith, R. J., Halloran, B. A., Day, T. J., Kelly, D. R., & Prince, L. S. (2007). FGF-10 is decreased in bronchopulmonary dysplasia and suppressed by Toll-like receptor activation. *American Journal of Physiology - Lung Cellular and Molecular Physiology*, *292*(2). https://doi.org/10.1152/ajplung.00329.2006

Berkelhamer, S. K., Mestan, K. K., & Steinhorn, R. (2018). An update on the diagnosis and management of bronchopulmonary dysplasia (BPD)-associated pulmonary hypertension. In *Seminars in Perinatology* (Vol. 42, Issue 7, pp. 432–443). W.B. Saunders. https://doi.org/10.1053/j.semperi.2018.09.005

Bhatt, A. J., Pryhuber, G. S., Huyck, H., Watkins, R. H., Metlay, L. A., & Maniscalco, W. M. (2001). Disrupted pulmonary vasculature and decreased vascular endothelial growth factor, Flt-1, and TIE-2 in human infants dying with bronchopulmonary dysplasia. *American journal of respiratory and critical care medicine*, *164*(10 Pt 1), 1971–1980. https://doi.org/10.1164/ajrccm.164.10.2101140

Bui, C. B., Pang, M. A., Sehgal, A., Theda, C., Lao, J. C., Berger, P. J., Nold, M. F., & Nold-Petry, C. A. (2017). Pulmonary hypertension associated with bronchopulmonary dysplasia in preterm infants. In *Journal of Reproductive Immunology* (Vol. 124, pp. 21–29). Elsevier Ireland Ltd. https://doi.org/10.1016/j.jri.2017.09.013

Chao, C. M., Moiseenko, A., Kosanovic, D., Rivetti, S., El Agha, E., Wilhelm, J., Kampschulte, M., Yahya, F., Ehrhardt, H., Zimmer, K.-P., Barreto, G., Rizvanov, A. A., Schermuly, R. T., Reiss, I., Morty, R. E., Rottier, R. J., Bellusci, S., & Zhang, J.-S. (2019). Impact of Fgf10 deficiency on pulmonary vasculature

formation in a mouse model of bronchopulmonary dysplasia. *Human Molecular Genetics*, *28*(9), 1429–1444. https://doi.org/10.1093/hmg/ddy439

Chao, C. M., Chong, L., Chu, X., Shrestha, A., Behnke, J., Ehrhardt, H., Zhang, J., Chen, C., & Bellusci, S. (2020). Targeting Bronchopulmonary Dysplasia-Associated Pulmonary Hypertension (BPD-PH): Potential Role of the FGF Signaling Pathway in the Development of the Pulmonary Vascular System. In *Cells* (Vol. 9, Issue 8). NLM (Medline). https://doi.org/10.3390/cells9081875

Chao, C. M., Yahya, F., Moiseenko, A., Tiozzo, C., Shrestha, A., Ahmadvand, N., El Agha, E., Quantius, J., Dilai, S., Kheirollahi, V., Jones, M., Wilhem, J., Carraro, G., Ehrhardt, H., Zimmer, K. P., Barreto, G., Ahlbrecht, K., Morty, R. E., Herold, S., … Bellusci, S. (2017). Fgf10 deficiency is causative for lethality in a mouse model of bronchopulmonary dysplasia. *Journal of Pathology*, *241*(1), 91–103. https://doi.org/10.1002/path.4834

Dankhara, N., Holla, I., Ramarao, S., & Kalikkot Thekkeveedu, R. (2023). Bronchopulmonary Dysplasia: Pathogenesis and Pathophysiology. *Journal of Clinical Medicine*, *12*(13). https://doi.org/10.3390/jcm12134207

David Surate Solaligue, X. E., José Alberto Rodríguez-Castillo, X., Katrin Ahlbrecht, X., Rory Morty, X. E., & Solaligue, S. DE. (2017). Recent advances in our understanding of the mechanisms of late lung development and bronchopulmonary dysplasia. *Am J Physiol Lung Cell Mol Physiol*, *313*, 1101–1153. https://doi.org/10.1152/ajplung

El-saie, A., Varghese, N. P., Webb, M. K., Villafranco, N., Gandhi, B., Guaman, M. C., & Shivanna, B. (2024). *Hypertension : An Updated Review*. *47*(6), 1–19. https://doi.org/10.1016/j.semperi.2023.151817.Bronchopulmonary

El Agha, E., Herold, S., Alam, D. Al, Quantius, J., MacKenzie, B. A., Carraro, G., Moiseenko, A., Chao, C. M., Minoo, P., Seeger, W., & Bellusci, S. (2014). Fgf10-positive cells represent a progenitor cell population during lung development and postnatally. *Development (Cambridge)*, *141*(2), 296–306. https://doi.org/10.1242/dev.099747

Finch, P. W., Mark Cross, L. J., Mcauley, D. F., & Farrell, C. L. (2013). Palifermin for the protection and regeneration of epithelial tissues following injury: New findings in basic research and pre-clinical models. *Journal of Cellular and Molecular Medicine*, *17*(9), 1065–1087. https://doi.org/10.1111/jcmm.12091

Hadzic, S., Wu, C. Y., Gredic, M., Pak, O., Loku, E., Kraut, S., Kojonazarov, B.,

Wilhelm, J., Brosien, M., Bednorz, M., Seimetz, M., Günther, A., Kosanovic, D., Sommer, N., Warburton, D., Li, X., Grimminger, F., Ghofrani, H. A., Schermuly, R. T., … Weissmann, N. (2023). Fibroblast growth factor 10 reverses cigarette smoke- and elastase-induced emphysema and pulmonary hypertension in mice. *The European Respiratory Journal*, *62*(5). https://doi.org/10.1183/13993003.01606-2022

Haggie, S., Robinson, P., Selvadurai, H., & Fitzgerald, D. A. (2020). Bronchopulmonary dysplasia: A review of the pulmonary sequelae in the post-surfactant era. *Journal of Paediatrics and Child Health*, *56*(5), 680–689. https://doi.org/10.1111/jpc.14878

Hansmann, G., Sallmon, H., Roehr, C. C., Kourembanas, S., Austin, E. D., & Koestenberger, M. (2021). Pulmonary hypertension in bronchopulmonary dysplasia. In *Pediatric Research* (Vol. 89, Issue 3, pp. 446–455). Springer Nature. https://doi.org/10.1038/s41390-020-0993-4

Hou, W., Yu, B., Li, Y., Yan, X., Su, Q., Fang, X., Zhou, X., & Yu, Z. (2024). PC (16:0/14:0) ameliorates hyperoxia-induced bronchopulmonary dysplasia by upregulating claudin-1 and promoting alveolar type II cell repair. *International Journal of Biochemistry and Cell Biology*, *172*(May). https://doi.org/10.1016/j.biocel.2024.106587

Jobe, A. H., & Bancalari, E. (2001). Bronchopulmonary dysplasia. *American journal of respiratory and critical care medicine*, *163*(7), 1723–1729. https://doi.org/10.1164/ajrccm.163.7.2011060

Jones, M. R., Chong, L., & Bellusci, S. (2021). Fgf10/Fgfr2b Signaling Orchestrates the Symphony of Molecular, Cellular, and Physical Processes Required for Harmonious Airway Branching Morphogenesis. In *Frontiers in Cell and Developmental Biology* (Vol. 8). Frontiers Media S.A. https://doi.org/10.3389/fcell.2020.620667

Jones, M. R., Dilai, S., Lingampally, A., Chao, C. M., Danopoulos, S., Carraro, G., Mukhametshina, R., Wilhelm, J., Baumgart-Vogt, E., Al Alam, D., Chen, C., Minoo, P., Zhang, J. S., & Bellusci, S. (2019). A comprehensive analysis of fibroblast growth factor receptor 2b signaling on epithelial tip progenitor cells during early mouse lung branching morphogenesis. *Frontiers in Genetics*, *10*(JAN). https://doi.org/10.3389/fgene.2018.00746

Kalikkot Thekkeveedu, R., Guaman, M. C., & Shivanna, B. (2017). Bronchopulmonary

dysplasia: A review of pathogenesis and pathophysiology. In *Respiratory Medicine* (Vol. 132, pp. 170–177). W.B. Saunders Ltd. https://doi.org/10.1016/j.rmed.2017.10.014

Lazarus, A., Del-Moral, P. M., Ilovich, O., Mishani, E., Warburton, D., & Keshet, E. (2011). A perfusion-independent role of blood vessels in determining branching stereotypy of lung airways. *Development*, *138*(11), 2359–2368. https://doi.org/10.1242/dev.060723

Maddaluno, L., Urwyler, C., & Werner, S. (2017). Fibroblast growth factors: Key players in regeneration and tissue repair. In *Development (Cambridge)* (Vol. 144, Issue 22, pp. 4047–4060). Company of Biologists Ltd. https://doi.org/10.1242/dev.152587

Marega, M., El-Merhie, N., Gökyildirim, M. Y., Orth, V., Bellusci, S., & Chao, C. M. (2023). Stem/Progenitor Cells and Related Therapy in Bronchopulmonary Dysplasia. *International Journal of Molecular Sciences*, *24*(13). https://doi.org/10.3390/ijms241311229

Mehler, K., Cate, F. E. U. Ten, Keller, T., Bangen, U., Kribs, A., & Oberthuer, A. (2017). An Echocardiographic Screening Program Helps to Identify Pulmonary Hypertension in Extremely Low Birthweight Infants with and without Bronchopulmonary Dysplasia: A Single-Center Experience. *Neonatology*, *113*(1), 81–88. https://doi.org/10.1159/000480694

Mourani, P. M., & Abman, S. H. (2013). Pulmonary vascular disease in bronchopulmonary dysplasia: Pulmonary hypertension and beyond. In *Current Opinion in Pediatrics* (Vol. 25, Issue 3, pp. 329–337). https://doi.org/10.1097/MOP.0b013e328360a3f6

Mourani, P. M., Sontag, M. K., Younoszai, A., Miller, J. I., Kinsella, J. P., Baker, C. D., Poindexter, B. B., Ingram, D. A., & Abman, S. H. (2015). Early pulmonary vascular disease in preterm infants at risk for bronchopulmonary dysplasia. *American Journal of Respiratory and Critical Care Medicine*, *191*(1), 87–95. https://doi.org/10.1164/rccm.201409-1594OC

Neumann, R. P., Schulzke, S. M., Pohl, C., Wellmann, S., Metze, B., Minke, A. K., Boos, V., Barikbin, P., Bührer, C., & Czernik, C. (2021). Right ventricular function and vasoactive peptides for early prediction of bronchopulmonary dysplasia. *PLoS ONE*, *16*(9 September). https://doi.org/10.1371/journal.pone.0257571

Northway, W. H. J., Rosan, R. C., & Porter, D. Y. (1967). Pulmonary disease following respirator therapy of hyaline-membrane disease. Bronchopulmonary dysplasia. *The New England Journal of Medicine*, *276*(7), 357–368. https://doi.org/10.1056/NEJM196702162760701

Ochoa-Espinosa, A., & Affolter, M. (2012). Branching morphogenesis: From cells to organs and back. *Cold Spring Harbor Perspectives in Biology*, *4*(10), 1–14. https://doi.org/10.1101/cshperspect.a008243

Ohuma, E. O., Moller, A. B., Bradley, E., Chakwera, S., Hussain-Alkhateeb, L., Lewin, A., Okwaraji, Y. B., Mahanani, W. R., Johansson, E. W., Lavin, T., Fernandez, D. E., Domínguez, G. G., de Costa, A., Cresswell, J. A., Krasevec, J., Lawn, J. E., Blencowe, H., Requejo, J., & Moran, A. C. (2023). National, regional, and global estimates of preterm birth in 2020, with trends from 2010: a systematic analysis. *The Lancet*, *402*(10409), 1261–1271. https://doi.org/10.1016/S0140-6736(23)00878-4

Prudovsky, I. (2021). Cellular mechanisms of fgf-stimulated tissue repair. In *Cells* (Vol. 10, Issue 7). MDPI. https://doi.org/10.3390/cells10071830

Ramasamy, S. K., Mailleux, A. A., Gupte, V. V., Mata, F., Sala, F. G., Veltmaat, J. M., Del Moral, P. M., De Langhe, S., Parsa, S., Kelly, L. K., Kelly, R., Shia, W., Keshet, E., Minoo, P., Warburton, D., & Bellusci, S. (2007). Fgf10 dosage is critical for the amplification of epithelial cell progenitors and for the formation of multiple mesenchymal lineages during lung development. *Developmental Biology*, *307*(2), 237–247. https://doi.org/10.1016/j.ydbio.2007.04.033

Schittny, J. C. (2017). Development of the lung. In *Cell and Tissue Research* (Vol. 367, Issue 3, pp. 427–444). Springer Verlag. https://doi.org/10.1007/s00441-016-2545-0

Scott, C. L., Walker, D. J., Cwiklinski, E., Tait, C., Tee, A. R., & Land, S. C. (2010). Control of HIF-1α and vascular signaling in fetal lung involves cross talk between mTORC1 and the FGF-10/FGFR2b/Spry2 airway branching periodicity clock. *American Journal of Physiology - Lung Cellular and Molecular Physiology*, *299*(4). https://doi.org/10.1152/ajplung.00348.2009

Sehgal, A., Gwini, S. M., Menahem, S., Allison, B. J., Miller, S. L., & Polglase, G. R. (2019). Preterm growth restriction and bronchopulmonary dysplasia: the vascular hypothesis and related physiology. *Journal of Physiology*, *597*(4), 1209–1220. https://doi.org/10.1113/JP276040

Siffel, C., Kistler, K. D., Lewis, J. F. M., & Sarda, S. P. (2021). Global incidence of

bronchopulmonary dysplasia among extremely preterm infants: a systematic literature review. *Journal of Maternal-Fetal and Neonatal Medicine*, *34*(11), 1721–1731. https://doi.org/10.1080/14767058.2019.1646240

Taghizadeh, S., Chao, C. M., Guenther, S., Glaser, L., Gersmann, L., Michel, G., Kraut, S., Goth, K., Koepke, J., Heiner, M., Vazquez-Armendariz, A. I., Herold, S., Samakovlis, C., Weissmann, N., Ricci, F., Aquila, G., Boyer, L., Ehrhardt, H., Minoo, P., … Rivetti, S. (2022). FGF10 Triggers De Novo Alveologenesis in a Bronchopulmonary Dysplasia Model: Impact on Resident Mesenchymal Niche Cells. *Stem Cells*, *40*(6), 605–617. https://doi.org/10.1093/stmcls/sxac025

Thébaud, B., Goss, K. N., Laughon, M., Whitsett, J. A., Abman, S. H., Steinhorn, R. H., Aschner, J. L., Davis, P. G., McGrath-Morrow, S. A., Soll, R. F., & Jobe, A. H. (2019). Bronchopulmonary dysplasia. In *Nature Reviews Disease Primers* (Vol. 5, Issue 1). Nature Publishing Group. https://doi.org/10.1038/s41572-019-0127-7

Thébaud, B., Ladha, F., Michelakis, E. D., Sawicka, M., Thurston, G., Eaton, F., Hashimoto, K., Harry, G., Haromy, A., Korbutt, G., & Archer, S. L. (2005). Vascular endothelial growth factor gene therapy increases survival, promotes lung angiogenesis, and prevents alveolar damage in hyperoxia-induced lung injury: Evidence that angiogenesis participates in alveolarization. *Circulation*, *112*(16), 2477–2486. https://doi.org/10.1161/CIRCULATIONAHA.105.541524

Veith, C., Neghabian, D., Luitel, H., Wilhelm, J., Egemnazarov, B., Muntanjohl, C., Fischer, J. H., Dahal, B. K., Schermuly, R. T., Ghofrani, H. A., Grimminger, F., Fink, L., Kwapiszewska, G., Weissmann, N., & Sydykov, A. (2020). FHL-1 is not involved in pressure overload-induced maladaptive right ventricular remodeling and dysfunction. *Basic Research in Cardiology*, *115*(2). https://doi.org/10.1007/s00395-019-0767-5

Walker, D. J., & Land, S. C. (2018). Regulation of vascular signalling by nuclear Sprouty2 in fetal lung epithelial cells: Implications for co-ordinated airway and vascular branching in lung development. *Comparative Biochemistry and Physiology Part - B: Biochemistry and Molecular Biology*, *224*, 105–114. https://doi.org/10.1016/j.cbpb.2018.01.007

Yuan, H. S., Xiong, D. Q., Huang, F., Cui, J., & Luo, H. (2019). MicroRNA-421 inhibition alleviates bronchopulmonary dysplasia in a mouse model via targeting Fgf10. *Journal of Cellular Biochemistry*, *120*(10), 16876–16887. https://doi.org/10.1002/jcb.28945

Yuan, T., Volckaert, T., Redente, E. F., Hopkins, S., Klinkhammer, K., Wasnick, R., Chao, C. M., Yuan, J., Zhang, J. S., Yao, C., Majka, S., Stripp, B. R., Günther, A., Riches, D. W. H., Bellusci, S., Thannickal, V. J., & De Langhe, S. P. (2019). FGF10-FGFR2B Signaling Generates Basal Cells and Drives Alveolar Epithelial Regeneration by Bronchial Epithelial Stem Cells after Lung Injury. *Stem Cell Reports*, *12*(5), 1041–1055. https://doi.org/10.1016/j.stemcr.2019.04.003

11 List of publications

Taghizadeh, S., Chao, C. M., Guenther, S., Glaser, L., Gersmann, L., Michel, G., Kraut, S., Goth, K., Koepke, J., Heiner, M., Vazquez-Armendariz, A. I., Herold, S., Samakovlis, C., Weissmann, N., Ricci, F., Aquila, G., Boyer, L., Ehrhardt, H., Minoo, P., Bellusci, S., … Rivetti, S. (2022). FGF10 Triggers De Novo Alveologenesis in a Bronchopulmonary Dysplasia Model: Impact on Resident Mesenchymal Niche Cells. Stem cells (Dayton, Ohio), 40(6), 605–617. https://doi.org/10.1093/stmcls/sxac025

12 Ehrenwörtliche Erklärung

„Hiermit erkläre ich, dass ich die vorliegende Arbeit selbständig und ohne unzulässige Hilfe oder Benutzung anderer als der angegebenen Hilfsmittel angefertigt habe. Alle Textstellen, die wörtlich oder sinngemäß aus veröffentlichten oder nichtveröffentlichten Schriften entnommen sind, und alle Angaben, die auf mündlichen Auskünften beruhen, sind als solche kenntlich gemacht. Bei den von mir durchgeführten und in der Dissertation erwähnten Untersuchungen habe ich die Grundsätze guter wissenschaftlicher Praxis, wie sie in der „Satzung der Justus-Liebig-Universität Gießen zur Sicherung guter wissenschaftlicher Praxis“ niedergelegt sind, eingehalten sowie ethische, datenschutzrechtliche und tierschutzrechtliche Grundsätze befolgt. Ich versichere, dass Dritte von mir weder unmittelbar noch mittelbar geldwerte Leistungen für Arbeiten erhalten haben, die im Zusammenhang mit dem Inhalt der vorgelegten Dissertation stehen, und dass die vorgelegte Arbeit weder im Inland noch im Ausland in gleicher oder ähnlicher Form einer anderen Prüfungsbehörde zum Zweck einer Promotion oder eines anderen Prüfungsverfahrens vorgelegt wurde. Alles aus anderen Quellen und von anderen Personen übernommene Material, das in der Arbeit verwendet wurde oder auf das direkt Bezug genommen wird, wurde als solches kenntlich gemacht. Insbesondere wurden alle Personen genannt, die direkt und indirekt an der Entstehung der vorliegenden Arbeit beteiligt waren. Mit der Überprüfung meiner Arbeit durch eine Plagiatserkennungssoftware bzw. ein internetbasiertes Softwareprogramm erkläre ich mich einverstanden.“

_____ _____

Ort/Datum Unterschrift

13 Acknowledgements

First and foremost, I would like to express my sincere gratitude to my primary supervisor, Prof. Dr. Saverio Bellusci, for his continuous support and guidance throughout my doctoral research. I am also deeply thankful to my co-supervisors, Dr. Stefano Rivetti and PD Dr. med. Cho-Ming Chao, for their valuable advice, expertise, and encouragement during the course of my dissertation.

I would like to extend a special thanks to Kerstin Goth, technical assistant of the research group. Her dedication and experience have been essential to the success of this research.

I am grateful to all my colleagues in the research group and cooperative projects at the institute for their collaboration and support throughout this project. Working alongside such dedicated and knowledgeable individuals has been both inspiring and rewarding. I want to thank Dr. Simone Kraut for the echocardiographic measurements and Dr. med. Ying Dong for her thoughtful suggestions during the final phase of writing my dissertation.

I want to thank my friends from university, who have been an incredible source of support throughout my doctoral journey. Their encouragement and understanding during challenging moments helped me stay motivated and focused.

My heartfelt appreciation goes to my family, especially my parents, my sister, and Yan, for their unwavering love, patience, and belief in me throughout this journey. This dissertation would not have been possible without their support.

Finally, I want to express my gratitude to the mice used in my experiments. Their role in this study was invaluable, and I appreciate the care and ethical considerations taken in their use.